

Active Switching in Long Distance Quantum State Teleportation

Diplomarbeit

VON

Rainer Kaltenbaek

im

Oktober 2003

zur Erlangung des
Grades eines Magisters
in Naturwissenschaften

Durchgeführt am
Institut für Experimentalphysik,
Gruppe Quantum Experiments and the Foundations of Physics,
o. Univ. Prof. Dr. Anton Zeilinger,
Universität Wien.

Gefördert vom Fonds zur Förderung der wissenschaftlichen Forschung
Projekt Nr. SFB 015

Contents

1. Principles of quantum information and entanglement	1
1.1. Elements of classical information theory	1
1.1.1. Shannon entropy	1
1.1.2. Noisy channel coding theorem	2
1.2. Elements of quantum information theory	3
1.2.1. The qubit	4
1.2.2. Von Neumann entropy	4
1.3. Quantum entanglement and nonlocality	5
1.3.1. Entangled states	5
1.3.2. The EPR paradox	6
1.3.3. Nonlocality	8
1.3.4. Local hidden variable theories	8
1.3.5. Bell's inequalities	9
1.3.6. Loopholes	12
2. Quantum state teleportation	13
2.1. A classical equivalent to teleportation	13
2.2. Teleportation of an unknown quantum state	13
2.2.1. The no-cloning theorem	14
2.2.2. Bennett's scheme of teleportation	15
3. Long distance quantum state teleportation	19
3.1. General Setup	19
3.2. Alice's laboratory	22
3.2.1. Experimental Bell state analysis	22
3.2.2. Theory of SPDC	27
3.2.3. Experimental setup of SPDC as entanglement source	29
3.2.4. The laser system pumping the BBO	33
3.3. The classical channel	34
3.3.1. Transmitter and receiver	36
3.3.2. Link stability	37
3.3.3. The delay between classical and quantum channel	38
3.3.4. Coding Alice's information for transmission on the classical channel	42
3.4. The quantum channel	44
3.5. Bob's laboratory	45
4. Hardware implementation of an actively triggered unitary transformation	49
4.1. Optical retarders as unitary transformations	49

4.2. The Pockels effect	50
4.3. Specifications of the Pockels cell	52
4.4. Setting up the Pockels cell as a fast phase switch	54
4.4.1. Isogyre Patterns	54
4.4.2. The experimental scheme	57
4.4.3. Specifications of the Pockels cell in static mode	58
4.5. Switching the Pockels cell	59
4.5.1. Switching high voltages on a short timescale	60
4.5.2. The switching behavior of the Pockels cell	61
5. Prospect and summary	73
A. Specifications	75
A.1. Fast high voltage transistor switch	75
A.2. Microwave link	75
A.2.1. Transmitter unit	76
A.2.2. Receiver unit	77
B. Labview programs	79
B.1. Scanning the switching process of the Pockels cell	79
B.2. Measuring the time delay between classical and quantum channel	79
Bibliography	81

Introduction

One of the most controversial implications of quantum mechanics are the non-local properties of entangled states. In 1935 Erwin Schrödinger stated[43]:

I would not call that one but rather the characteristic trait of quantum mechanics, the one that enforces its entire departure from classical lines of thought.

The seeming paradox of these states led to one of the most fruitful discussions (started by the EPR-paper[20] in 1935) in the modern history of physics, which builds the basis of quantum information - today, one of the fastest growing branches in physics.

Another great step in the development of this field were the theorems of John Bell. His famous inequalities provide a way to decide experimentally between quantum mechanics and local hidden variable theories.

Before the eighties of the last century these theories and thoughts could only be "tested" in gedankenexperiments. But when it became possible to realize these experiments, they were perfectly conform with quantum mechanics.

Since then a lot of work has been invested into finding the properties and also applications of entangled states like quantum cryptography, quantum dense coding, quantum teleportation combined in the familiar quotation "quantum communication".

While during the nineties, physicists were mainly concerned in doing proof-of-principle experiments related to quantum communication, today more and more experiments are done to improve the efficiency and range of schemes that are already known to work.

One out of these last group of experiments is long distance quantum state teleportation at our Danube-laboratory, where we are trying to realize teleportation over long distances and to implement active switching, which was the central part of my work.

RAINER KALTENBAEK

Vienna, Austria
December, 2002

1. Principles of quantum information and entanglement

During the last decades it has become more and more apparent that many physical principals can be expressed in terms of distributing and gathering information. Great efforts are currently invested into finding an information theoretical basis on which to foot today's physics, especially quantum mechanics.

While classical information theory as introduced by Shannon (see section 1.1 below) is an established theory, quantum information theory is still in its infancy. Any attempt to explain quantum mechanical principles on an information theoretical basis is up to now mostly educated guessing.

1.1. Elements of classical information theory

In 1948 C. E. Shannon published his historical paper "A Mathematical Theory of Communication" which was first published in two parts[44]. This paper represents the foundation of modern information theory. Its fundamental unit is the **bit**.

Shannon's investigations were led by two basic questions:

- how much redundancy does a given message contain, i.e. what is the minimum number of bits a message can be compressed to without loosing any information?
- at which rate can one communicate reliably over a noisy channel, i.e. how much redundancy must be incorporated into a message to protect it against errors?

To answer the first question one has to quantify the complexity of a given message. Clearly, the easier it is to guess the next letter of a message, the less information it contains; i.e. the uncertainty of each letter is a measure for the amount of information contained. Shannon thus recognized the entropy to be the adequate measure of information (see section 1.1.1).

The second question is strongly connected to the question of which is the optimal encoding ensuring reliable communication over a noisy channel (see section 1.1.2).

1.1.1. Shannon entropy

A message is a string consisting of n letters. For a binary string these are taken out of an alphabet of two letters $\{a_1, a_2\}$, where letter a_1 appears with

probability p and a_2 with probability $1 - p$. Then, for large n a typical string will contain about np letters a_1 and about $(1 - p)n$ letters a_2 .

Therefore, the number of strings one can build out of np a_1 's and $(1 - p)n$ a_2 's gives us the number of typical strings:

$$\binom{n}{np} \quad (1.1)$$

Using the approximation $\log n! = n \log n - n + O(\log n)$ we obtain¹

$$\log \binom{n}{np} \simeq nH(p), \quad (1.2)$$

where

$$H(p) = -p \log p - (1 - p) \log (1 - p). \quad (1.3)$$

Hence, the number of typical strings of length n is of order $2^{nH(p)}$ which means that we need on average $nH(p)$ bits to encode such a typical string.

This argument can be easily generalized to strings composed of letters out of an alphabet of k letters, where letter x occurs with probability $p(x)$. Then the number of typical strings is of order

$$\frac{n!}{\prod_x (np(x))!} \simeq 2^{nH(X)}, \quad (1.4)$$

where we have used the *Shannon entropy*

$$H(X) = - \sum_x p(x) \log p(x) \quad (1.5)$$

of the ensemble $X = \{x, p(x)\}$.

To summarize these results one could say that on average one needs $H(X)$ bits to encode one letter out of an ensemble X , where the letter shall be part of a string whose length n approaches infinity.

1.1.2. Noisy channel coding theorem

Suppose we transmit a letter x out of an ensemble X to someone else who will receive some corresponding y out of an ensemble Y . If the channel used for transmission is noiseless, $H(X)$ will be equal to $H(Y)$; i.e. no information is lost.

If the channel is noisy, how much uncertainty is left in x when y is known? This is given by

$$H(X|Y) = \langle -\log p(x|y) \rangle, \quad (1.6)$$

where $p(x|y)$ is the probability that x has been sent when y is received. Using Bayes' rule it is given by

$$p(x|y) = \frac{p(y|x)p(x)}{p(y)}. \quad (1.7)$$

¹All logarithms we use are of base 2.

From this it follows that

$$H(X|Y) = H(X, Y) - H(Y) \quad (1.8)$$

and

$$H(Y|X) = H(X, Y) - H(X), \quad (1.9)$$

where $H(X, Y)$ is given by

$$H(X, Y) = \langle -\log p(x, y) \rangle, \quad (1.10)$$

$\log p(x, y)$ being the probability for having x on one and y on the other side. If these two events were independent of each other, we would get .

So by receiving a letter out of Y on average one gains

$$\begin{aligned} I(X; Y) &\equiv H(X) - H(X|Y) \\ &= H(Y) - H(Y|X) \\ &= H(X) + H(Y) - H(X, Y) \end{aligned} \quad (1.11)$$

bits of information about the original letter out of X . $I(X; Y)$ is called *mutual information* and describes the information transferred on average over a channel by sending one letter. In the case of a completely noisy channel, the letters received (y) will be totally independent of the letters sent. Therefore we get $\log p(x, y) = \log [p(x)p(y)]$, which results in $H(X|Y) = H(X)$ and $H(Y|X) = H(Y)$. From this we see that $I(X; Y) = 0$, as it should be.

As $I(X; Y)$ still depends on the special distribution of probabilities in the alphabet X one chooses, it is not a direct measure for the quality of the channel. The real *channel capacity* - the maximum number of bits one can transfer by sending one letter is given by

$$C \equiv \max_{\{p(x)\}} I(X; Y), \quad (1.12)$$

which is now independent of the special alphabet in use, and is only determined by the channel's properties.

1.2. Elements of quantum information theory

In 1959 Richard P. Feynman gave a talk [23] on the annual meeting of the American Physical Society concerning the possibility of miniaturizing machines and storage devices down to the scale of several atoms. Carrying on with this argument, one naturally arrives at the point where one bit of information is stored in one particle using its quantum state to encode the information.

At this point the procedure does not only involve simple miniaturization anymore. One enters a whole new realm in which one has to take quantum mechanical laws into account explicitly.

1.2.1. The qubit

The natural smallest unit of information in classical information theory is the bit given by a value of 0 or 1. In classical information theory these two values represent two mutually exclusive alternatives. So it is **either 0 or 1**.

If one wants to encode a bit of information in a quantum state, the natural choice is a two-level quantum system described by a state vector in a two dimensional Hilbert space. 0 is now represented by the state being $|0\rangle$, and 1 by the state $|1\rangle$, where $\langle 0|1\rangle = 0$. Therefore, by preparing a quantum system in state $|0\rangle$ or $|1\rangle$ it is possible to encode one bit of classical information in the system. This is at the same time the maximum amount of classical information possible to encode in a single qubit.

The interesting thing is that a quantum system can of course also be in a superposition of the two states:

$$|\Psi\rangle = \alpha|0\rangle + \beta|1\rangle, \quad (1.13)$$

where $|\alpha|^2 + |\beta|^2 = 1$. Due to its natural relation to the classical bit and its quantum mechanical properties, such a two-level system is called a **qubit**. It is the smallest unit of information in quantum information theory as there is no simpler non-trivial system than the two-level system.

Another important aspect of qubits is the possibility of them being in a mixed state; i.e. a statistical mixture of several states. In general any mixed qubit state can be written as:

$$\rho = \frac{1}{2}(1 + \vec{r} \cdot \vec{\sigma}), \quad (1.14)$$

where $\vec{\sigma}$ denotes the vector of Pauli matrices. Using this general definition for the density operator ρ of a single qubit, we can also adapt the usual definition of a pure state to our notation. A qubit state is pure if and only if the following holds:

$$\text{tr}(\rho^2) = 1 \iff |\vec{r}| = 1. \quad (1.15)$$

For any mixed state both, the trace of ρ^2 and the modulus of \vec{r} will be less than unity.

1.2.2. Von Neumann entropy

As we saw in section 1.1.1 it is relatively easy to find a measure for classical information contained in a string composed of letters out of a given alphabet. This can be generalized to quantum information.

Suppose we want to encode a string using quantum states $\{|a_1\rangle, |a_2\rangle, \dots\}$ as letters, where $\langle a_m|a_n\rangle = \delta_{mn}$. Each letter ($|a_k\rangle\langle a_k|$) shall be appearing with the probability p_k ($\sum_k p_k = 1$ and $\forall k : p_k \geq 0$).

As the receiver will have no further information about the message sent to him, every letter he receives will be a mixture of quantum states out of the ensemble $X = \{p_k, |a_k\rangle\}$ described by the density operator

$$\rho = \sum_k p_k |a_k\rangle\langle a_k|. \quad (1.16)$$

This is just classical communication encoded in quantum systems. The special properties of quantum mechanics do not occur here. Therefore, the information transmitted on average per letter is just the Shannon entropy $H(X) = -\sum_k p_k \log p_k$. But that also means that the amount of our ignorance about the single letter (the mixed quantum state) is given by that entropy.

Now, let us define the **von Neumann entropy**

$$S(\rho) \equiv -\text{tr}(\rho \log \rho). \quad (1.17)$$

This entropy proves to have just the properties we would be expecting of an adequate measure for quantum information:

- if ρ is pure, $S(\rho) = 0$, as then only one letter would be used, not bearing any information
- $S(\rho)$ is maximal for a totally mixed state, as in this case the uncertainty about which letter is going to arrive next is largest
- for a general state $\rho = \sum_k p_k |a_k\rangle\langle a_k|$ we get $H(X) \geq S(\rho)$ for the ensemble $X = \{p_k, |a_k\rangle\}$, with equality if and only if the states $|a_k\rangle$ are mutually orthogonal

The last point should be emphasized as the choice of non-orthogonal states implies a loss of distinguishability, i.e. even if there is no noise in the transmission of the message one cannot distinguish two letters with certainty if the corresponding quantum states are not orthogonal.

1.3. Quantum entanglement and nonlocality

Quantum entanglement stands at the very heart of today's efforts in the field of quantum communication. The most promising innovations in this new field of physics like quantum state teleportation[6, 14], quantum cryptography[21, 5] and quantum super-dense coding[7] all base on the use of quantum entanglement.

Another great interest in quantum entanglement originates in its implications for the foundations of physics and its central role in the development of quantum information theory.

1.3.1. Entangled states

Consider two distinct, well separated quantum systems and let these quantum systems be represented by qubit states $|\chi_1\rangle$ and $|\chi_2\rangle$ in the according Hilbertspaces H_1 and H_2 . Then, the state describing the overall system will be given by the tensor product

$$|\chi_{12}\rangle = |\chi_1\rangle \otimes |\chi_2\rangle, \quad (1.18)$$

which is a state in the composite Hilbert space $H_{12} = H_1 \otimes H_2$. Up to now there is nothing special about this, it is just a way to talk about both quantum

systems at once. But if we allow the two systems to interact in a general way with each other, the composite state $|\chi_{12}\rangle$ will evolve to a different state $|\chi'_{12}\rangle$, which in general will be no longer a product state, i.e. it cannot be written in the form of equ. 1.18, it is *nonseparable*.

These states have an interesting property. If we perform a measurement on only one part of the system, the nonseparable state will be projected in a separable one and, therefore, the resulting state of the second part of the system will depend on the actual outcome of the measurement on the first part.

A good example is the following state

$$\frac{1}{\sqrt{2}} (|A\rangle_1 |B\rangle_2 + |B\rangle_1 |A\rangle_2), \quad (1.19)$$

where the states A and B shall be orthogonal to each other. If we perform a measurement on particle one given by the operator $|A\rangle\langle A|_1 - |B\rangle\langle B|_1$, we will get either outcome +1 or outcome -1 with equal probability. But depending on the outcome we get, the overall state will either be projected on $|A\rangle_1 |B\rangle_2$ or $|B\rangle_1 |A\rangle_2$. If we now perform an equivalent measurement on particle 2, we will know for certain its outcome, if we know the outcome of the previous measurement. The results of the measurements are somehow entangled, they are not independent of each other. Since this is an intrinsic property of states like the one under consideration, we call them entangled states. The term *entangled* was first introduced by E. Schrödinger[43]:

When two systems, of which we know the states by their respective representatives, enter into temporary physical interaction[...], then they can no longer be described in the same way as before, viz. by endowing each of them with a representative of its own[...]. By the interaction the two representatives (or ψ -functions) have become entangled.

The fact, that it is possible to predict the result of a measurement on a particle with certainty, that may be indefinitely far away, has led to excited discussions and interesting discoveries, which will partly be covered in the following.

1.3.2. The EPR paradox

In their 1935 paper [20] Einstein, Podolsky and Rosen (EPR) tried to prove that quantum mechanics is *incomplete* by exploiting the special properties of an entangled state. To elucidate this, we will sketch their argument.

EPR's argument

It bases upon the following definition of terms

- a physical theory can be called *complete* if every *element of physical reality* has a counterpart in the physical theory
- a physical quantity is said to have a corresponding *element of physical reality* if, without in any way disturbing a system, we can predict with certainty (i.e. with probability equal to unity) the value of this quantity

Quantum mechanics tells us that two complementary observables like position and momentum cannot be measured accurately at the same time. If one were known precisely, we would be totally ignorant about the second. Additionally, measurement of one such observable destroys information about the second observable. EPR conclude that this allows only two alternative interpretations:

1. the quantum mechanical description of the physical world is incomplete
2. the two quantities corresponding to the complementary observables cannot have simultaneous reality

To find which of these two interpretations is correct, they investigate the properties of a two particle state entangled in position and momentum. They argue that by measuring either the momentum or the position of one particle one knows the momentum or the position of the other particle with certainty.

Hence, in one case the momentum of the second particle has to be an element of reality, while in the other case the position of the second particle has to be an element of reality. But, as long as the experimenter decides fast enough which measurement to perform or as long as the particles are separated far enough, the experimenters decision what to measure on the first particle cannot have any influence on what is reality for the second particle. Therefore, EPR conclude, both the momentum and the position of the second particle have to be elements of reality simultaneously.

This is in direct contradiction to the second possibility mentioned above. Therefore, the first possibility must be correct: quantum mechanics is incomplete.

The counter-argument

A few months later, in answer to EPR's paper on quantum mechanics Nils Bohr [12] states that EPR have made an ill assumption right in the beginning of their argument where they state "[...] without in any way disturbing a system [...]" . Bohr points out that it is *not* possible to assume that the system is not disturbed by the measurement of the first particle. This is due to the fact that for measuring the momentum or the position of the particle an appropriate measurement device has to be either rigidly connected with the other parts of the apparatus (with the aid of which the experiment is performed) or their relative velocities have to be known very accurately. Thus, due to the nature of position and momentum measurements the performance of a measurement will have an according influence on the apparatus blurring either its position or momentum in correspondence to the measurement performed. Thereby, the system is disturbed in contradiction to EPR's basic assumption mentioned above.

This disturbance of the apparatus influences "[...]" the very conditions which define the possible types of predictions regarding the future behavior of the system [...] [12]. As these conditions are a necessity in the description of any phenomenon to which the term "physical reality" can be properly attached, EPR's argument does not justify their conclusion that quantum mechanical description is essentially incomplete.

1.3.3. Nonlocality

Though the original EPR argument has been "disarmed" by Bohr, the interest in entangled states did not falter. While they could not be used to show any inconsistency of quantum mechanics, they can be used on the contrary to confirm the fundament of quantum mechanics.

Some years after EPR D. Bohm found a simpler realization of entangled states[11]. He considered a molecule of total spin zero, consisting of two atoms, each of spin one-half. Therefore the molecule is in a spin singlet state:

$$\psi = \frac{1}{\sqrt{2}}(\psi_+(1)\psi_-(1) - \psi_-(1)\psi_+(2)), \quad (1.20)$$

where $\psi_{\pm}(i)$ corresponds to a wave function of the atomic state in which particle i has spin $\pm\hbar/2$. If the two atoms are then separated by a method not influencing the total spin, their spin state will remain in the singlet state and can more also be written in the more familiar form

$$|\Psi\rangle = \frac{1}{\sqrt{2}}(|\uparrow\rangle_1|\downarrow\rangle_2 - |\downarrow\rangle_1|\uparrow\rangle_2). \quad (1.21)$$

This is a maximally entangled state much of the same form as the state indicated in equ. 1.19.

It has similar properties to the state introduced by EPR. But while their original state is not realizable experimentally this state can be prepared quite easily. Especially, the seemingly nonlocal properties of the state are the same. If for example on one particle the spin along the z-axis is measured, the result will be either up or down with equal probability. Once this result is known, we can predict with 100% certainty the result of a measurement along the z-axis of the second particle; it will be the opposite.

While for quantum mechanics this result is obvious just from considering the state, a realist holding true to Einstein's locality runs into serious problems, as locality prohibits any interaction between spacelike separated events. The above measurements can be chosen to be separated this way but, nevertheless, are strongly correlated. From the quantum mechanical point of view the error in this is obvious: the two particles are not separated, they build one quantum mechanical system that corresponds in this "disconcerting" way when projected on the state of two separate particles. Of course this projection happens instantaneously but that does not matter as it happens in Hilbert space and not in the physical world.

Nevertheless, in conjunction with those correlations between two measurements, the term nonlocality can often be heard. This does not mean that quantum mechanics implies superluminal interactions but **only** that these correlations cannot be reproduced by any local realistic theory as will be discussed in the following.

1.3.4. Local hidden variable theories

Classical physics is an atomistic theory, it describes physical systems by separating it in its constituents. All the properties of the composed system can then be predicted from the properties of its constituents and their interaction.

Now, if one applies this view to a particle pair in an entangled state, the only way to describe the correlations of the particles in measurements, is to say that they interact with each other during the measurement process or that they have properties of their own that are in some way related through their common origin.

If we want to hold true to Einstein's locality, the cause of the correlations cannot be any interaction of the two systems, as their correlations appear in the usual way, even if the measurement processes are spacelike separated. Hence, we consider only *local hidden variable (LHV) theories*, which assume that every particle carries with it some hidden properties, determining the outcomes of all possible measurements, which could be performed on them. The hidden variables may be correlated in any possible way, but they are fixed to the particles; i.e. if the particles are spacelike separated, the two according sets of hidden variables will not be able to influence each other.

These theories attempt to reproduce the predictions of quantum mechanics while being based upon *local realistic* concepts and it is a most fundamental question if this could be possible even in principle. If it were, then quantum mechanics would just be a statistical theory of which we do not know the underlying principles, and its fundamental postulates would just be statements of our ignorance about those more fundamental principles².

1.3.5. Bell's inequalities

The discussion about the inconsistency of hidden variable theories with the predictions of quantum mechanics had its beginning shortly after quantum mechanics itself (e.g. [34]). These arguments against hidden variable theories were of a mathematical nature and based upon physically unrealistic postulates (for a survey of these proofs see [3]). It was John S. Bell who proposed a physically reasonable argument for the inconsistency of *local* hidden variable models with quantum mechanics [4]. He proved that no local hidden variable theory is able to reproduce quantum predictions. This is perfectly consistent with the fact that in 1952 D. Bohm published a hidden variable theory consistent with quantum predictions [9, 10] which is explicitly nonlocal.

In his argument, Bell considers a spin experiment performed by two parties on a twopartite entangled spin singlet state (see equ. 1.21) using Stern Gerlach (SG) apparatuses. Each of these apparatuses can be arbitrarily oriented in some direction and according to quantum mechanics in very case there are only two outcomes possible, which we will denote as +1 and -1. Additionally, if the SG measuring one particle is oriented in direction \vec{a} , and the other SG is oriented in direction \vec{b} , the expectation value for the product of the two measurement outcomes is given by quantum mechanics to be

$$E_{QM}(\vec{a}, \vec{b}) = -\vec{a} \cdot \vec{b}. \quad (1.22)$$

To see if local hidden variable theories are able to reproduce this prediction of quantum mechanics, he developed a very general mathematical model that

²This situation very much resembles the relation between classical thermodynamics and statistical mechanics.

contains any local hidden variable theory that could attempt to describe this experiment. Bell's model is based on assumptions, every local hidden variable theory has to fulfill:

- each particle carries with it a set of hidden variables denoted by a general parameter λ out of some parameter space Γ (this parameter represents all possible kinds of hidden variables; numbers, matrices, whole sets of functions, etc.).
- if the parties are spatially separated, the choice which measurement a party makes, has no influence on the outcome of the measurement the second party performs³. That means, the measurement outcomes are functions of λ and of the orientation of the according Stern-Gerlach apparatus: $A(\lambda, \vec{a})$ for one party and $B(\lambda, \vec{b})$ for the other.
- supposing the probability distribution of λ is $p(\lambda)$, the expectation value of measurements along \vec{a} and \vec{b} will be

$$E(\vec{a}, \vec{b}) = \int_{\Gamma} d\lambda p(\lambda) A(\lambda, \vec{a}) B(\lambda, \vec{b}). \quad (1.23)$$

Subsequently, Bell shows that no model of this type is able to reproduce quantum predictions for the spin singlet state. This is done by deriving an inequality which is fulfilled by all models of the type described above but can be violated by the predictions of quantum mechanics. Therefore, Bell concludes, local hidden variable theories are in general not able to reproduce quantum predictions in the case of this experiment.

Bell's argument requires perfect correlations and is therefore not applicable to the real experiment. However, the nature of the argument has been carried on by other physicists and has led to Bell type inequalities, paying attention to experimental imperfections. One of the best known inequalities of this type is the inequality by Clauser, Horne, Shimony and Holt (CHSH) inequality [18]. They consider an experiment as illustrated in fig. 1.1. Two parties (Alice and Bob) share a spin singlet state, each performing one of two possible measurements on their part of the state.

From the point of view of LHV theories, it is clear that as soon as the particles are separated from each other, the outcome of any measurement performed on them will be determined by the hidden variables. Hence, we can say if Alice performs measurement 1, she will get result A1, while if she performs measurement 2, she will get result A2. The same argument holds for Bob, so he too, has two possible measurement outcomes B1 and B2, depending on which measurement he actually performs⁴.

If we choose our measurements to have only two possible outcomes, we can denote them freely as +1 and -1. In this case, it follows that

$$|A1(B1 + B2) + A2(B1 - B2)| = 2, \quad (1.24)$$

³This ensures the local character of the model.

⁴All these results are of course dependent on the hidden variables.

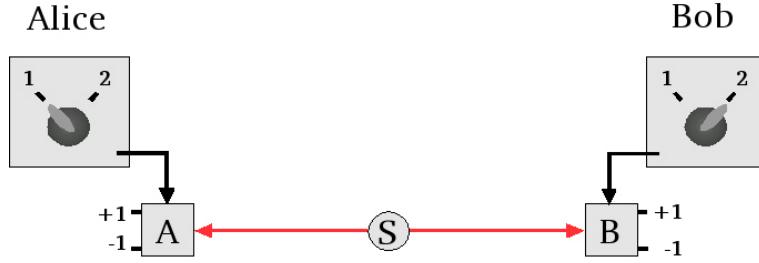


Figure 1.1.: In a Bell type experiment an entangled state is shared between two parties (indicated as Alice and Bob). Alice and Bob each randomly choose one out of two possible measurements to perform of their part of the entangled system. Each of the measurements has the two possible outcomes $+1$ and -1 . Due to the entanglement the measurement results of Alice and Bob will show correlations that cannot be reproduced by LHV theories.

as it is either $B_1+B_2 = \pm 2$ and $B_1-B_2 = 0$ or $B_1+B_2 = 0$ and $B_1-B_2 = \pm 2$. By averaging over many measurements, we get the following inequality:

$$|\langle A_1 \cdot B_1 \rangle + \langle A_1 \cdot B_2 \rangle + \langle A_2 \cdot B_1 \rangle - \langle A_2 \cdot B_2 \rangle| \leq 2. \quad (1.25)$$

If the performed spin measurements are only oriented in one plane, we can describe the measurements by angles $\alpha_1, \alpha_2, \beta_1$ and β_2 , where α 's are describing Alice's measurements and β 's Bob's measurements. Using these definitions, we can write the inequality in the more common form

$$|E(\alpha_1, \beta_1) + E(\alpha_1, \beta_2) + E(\alpha_2, \beta_1) - E(\alpha_2, \beta_2)| \leq 2, \quad (1.26)$$

where $E(\alpha_i, \beta_j)$ is the expectation value of Alice's and Bob's joint outcome for measurements i and j .

The advantage of this inequality is apparent, as it is based on experimental statistics while Bell's original inequality required the perfect correlations of maximally entangled quantum states. Additionally, the inequality's derivation is very general and can thus be applied to any experiment with two possible settings and two possible outcomes on each side.

By using the quantum mechanical expectation value $E(\alpha, \beta) = -\cos(\alpha - \beta)$ for SG measurements on a spin singlet state in 1.26, we obtain

$$|\cos(\alpha_1 - \beta_1) + \cos(\alpha_1 - \beta_2) + \cos(\alpha_2 - \beta_1) - \cos(\alpha_2 - \beta_2)| \leq 2. \quad (1.27)$$

For some choices of angles, however, this inequality will be violated, the violation being maximal for the angles $\alpha_1 = 0^\circ, \alpha_2 = 45^\circ, \beta_1 = 22.5^\circ$ and $\beta_2 = 67.5^\circ$. In this case we get

$$2\sqrt{2} \leq 2, \quad (1.28)$$

which is obviously wrong. Therefore, quantum mechanical predictions are in contradiction to local hidden variable theories and can thus not be reproduced

by them. This still leaves the question open if experimental results can be reproduced by LHV theories, but this has been shown in many experiments to be not the case⁵.

1.3.6. Loopholes

In order to derive strong Bell-type inequalities for LHV theories, one has to apply several assumptions:

- the detection probability of particles does not depend on their state, analysis of the particles before detection cannot increase the detection probability and the sum of detection probabilities behind a two-channel analyzer does not depend on its spatial direction
- the actually detected subensemble is a representative sample of the whole ensemble
- even if of two measurements (treated events in space-time) one could in principle influence the other without violating Einstein's locality, it is assumed that there is no such interaction

All of these points can be violated on purpose by LHV theories to circumvent being ruled out by Bell-type inequalities. Therefore these assumptions are regarded as so-called loopholes for LHV theories in Bell-type arguments. The first two points can generally be seen as a set of assumptions about the detection process and therefore the possibility to build a LHV theory to which Bell-type arguments do not apply is called the *detection loophole*.

The third point can be violated by assuming some subluminal interaction between the different measurements thereby reproduce quantum mechanical results (*locality loophole*).

Both of these loopholes were experimentally closed in separate experiments. The detection loophole was closed by Rowe et al. [41], the locality loophole in a first attempt by Aspect et al. [2] and finally by Weihs et al. [47].

⁵For a very complete list of these experiments see pages 33-44 in [48]

2. Quantum state teleportation

The idea of teleportation is the displacement of an object from one place to another without the object ever crossing the space in between.

Although it is certainly best known from science fiction movies and books, teleportation in this sense is still impossible to realize as far as we know today. But the term teleportation can also be appropriately applied to a more realistic process which will be discussed in this chapter: *the teleportation of a quantum state*.

2.1. A classical equivalent to teleportation

With the methods of classical physics, how could it be possible to teleport an object from place A to B? As the object itself cannot be sent, the best alternative is to send all information about the object from A to B. Then at place B this information can be used to reconstruct the object, while at A the original object is still existing. In principle, therefore, the classical equivalent to teleportation is nothing else but a copying machine. This way any number of copies of A could be produced. To make this protocol equivalent to teleportation, one would have to deliberately destroy the original object.

2.2. Teleportation of an unknown quantum state

Now, if we intend to teleport a quantum state from A to B the classical protocol described in the last section cannot be applied as can be easily seen.

Suppose the sender is given some quantum state to teleport. If he knows the state, teleporting it will pose no problem but it would be hard to call it teleportation. The sender would just have to share his knowledge with the receiver who would then prepare the state of a particle of the same type accordingly. Therefore, this protocol is rather a remote preparation of a state than real teleportation. Nevertheless, the accuracy of this protocol is limited, as a quantum state is in general described by at least two real numbers (for a qubit). To encode a real number one usually needs an infinite number of bits. Therefore, the accuracy of this scheme is limited by the number of bits that is allowed to be transferred.

If, on the other hand, the sender does not know the quantum state, he will be unable to determine it, as any measurement destroys the state measured and its result would in general just be a random value. This is a basic property of the quantum mechanical measurement process.

The only possible loophole would be to copy the quantum state very often, since a measurement on many identical systems can reveal the state of these

2. Quantum state teleportation

systems reasonably well and, asymptotically, even exactly. But this procedure is impossible due to the no-cloning theorem, which forbids the perfect copying of a single quantum state.

2.2.1. The no-cloning theorem

The no-cloning theorem tells us that an unknown quantum state cannot be exactly copied but only with a certain accuracy smaller than 100%[49]. The exact upper limit is still unknown and might well depend on the exact type of the cloning apparatus in use. It is clear, though, that there has to exist a certain upper limit, as cloning even if nonperfect would in principle allow superluminal transfer of information. To see this, suppose a typical Bell experiment as described in 1.3.5. By choosing her basis of measurement, Alice determines the basis of the state of Bob's particle. For instance, if she measures the spin in z-direction, Bob's particle will be projected either in the z-up or the z-down state, whereas if Alice measures in x-direction, Bob's particle will be projected accordingly. In a single shot measurement, Bob is not able to tell, which basis the particle's state is in. But if he was able to clone the particle an arbitrary number of times he could determine the state of his particle and therefore determine the basis, Alice has measured in. Thus, by choosing her basis accordingly, Alice could therefore code information this way with a velocity that would only be limited by the speed of Bob's measurement procedure. As the principle of causality prohibits superluminal transfer of information, the cloning of a quantum state has to be limited in a way to circumvent its possibility.

That perfect cloning is impossible can also be shown in a more formal way. For this we choose the original proof of Wootters and Zurek[49].

A quantum cloner would in principle have two inputs and two outputs. One input is the particle to be cloned, while the second input is a particle of the same type whose state is irrelevant¹. The two outputs would then be two identical particles.

Quantum mechanics tells us that the cloner is represented by a unitary transformation U_{Cloner} upon the two particles. Then, from the definition of the cloner it follows that it will copy any state we feed it with. For the states $|0\rangle$ and $|1\rangle$ this can be written as

$$U_{\text{Cloner}} : |0\rangle_1 |\alpha\rangle_2 \longrightarrow |0\rangle_1 |0\rangle_2 \quad (2.1)$$

and

$$U_{\text{Cloner}} : |1\rangle_1 |\alpha\rangle_2 \longrightarrow |1\rangle_1 |1\rangle_2, \quad (2.2)$$

where $|\alpha\rangle$ is the initial state of the second input particle.

Any other state, we might copy, can be written as a superposition $\alpha|0\rangle + \beta|1\rangle$ of the basis states $|0\rangle$ and $|1\rangle$. Now, if we want to clone such a superposition, due to equ. 2.1 and 2.2 we get:

$$U_{\text{Cloner}} : (\alpha|0\rangle_1 + \beta|1\rangle_1) |\alpha\rangle_2 \longrightarrow \alpha|0\rangle_1 |0\rangle_2 + \beta|1\rangle_1 |1\rangle_2, \quad (2.3)$$

¹Just like the blank sheet in a usual copier

while the thing we actually wanted to get is $(\alpha|0\rangle_1 + \beta|1\rangle_1)(\alpha|0\rangle_2 + \beta|1\rangle_2)$.

This shows that it is not possible to clone a single quantum state if it is unknown.

2.2.2. Bennett's scheme of teleportation

In 1993 Ch. Bennett et al [6] suggested a way to circumvent the no-cloning theorem while simultaneously opening the way for the teleportation of quantum states in the most original meaning. Their scheme bases upon the nature of quantum measurements, which has already been mentioned before in the context of the classical teleportation of a single quantum state. It is in principle applicable for systems of arbitrary dimensional Hilbert space. For simplicity, and because higher dimensional teleportation has not yet been performed, we shall concentrate on the teleportation of two-dimensional systems.

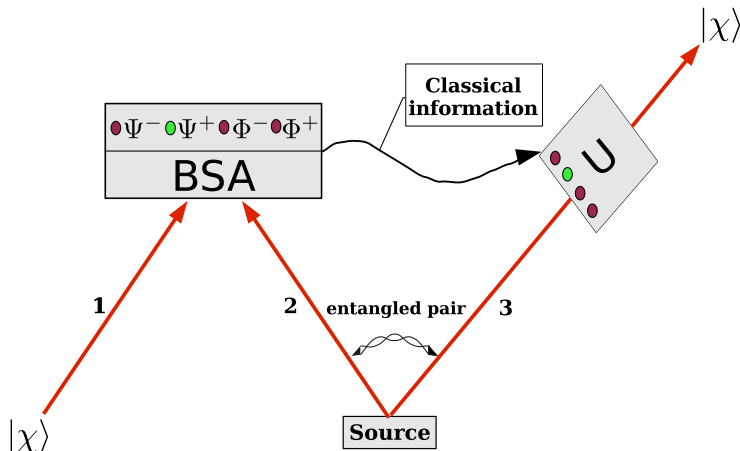


Figure 2.1.: Sender and receiver (Alice and Bob) share a maximally entangled pair. To teleport the state $|\chi\rangle$ of qubit 1, Alice performs a Bell state analysis (BSA) on particles 1 and 2. Particle 3 is thereby projected on a state $U_i|\chi\rangle$, where the unitary operator U_i depends on the outcome of the BSA. This outcome has to be sent to Bob via a classical channel. Bob then knows, which inverse unitary transformation to apply to transform the state of particle 3 back to $|\chi\rangle$.

Figure 2.1 shows the basic layout of this scheme. An entangled pair of particles (with indices 2 and 3) is shared between the sender and the receiver (Alice and Bob). For reasons of convenience the pair shall be in the singlet state

$$|\Psi_{23}^-\rangle = \frac{1}{\sqrt{2}}(|0\rangle_2|1\rangle_3 - |1\rangle_2|0\rangle_3) \quad (2.4)$$

like in equ. 1.21, whereas now the spins up and down have been replaced by more general 0s and 1s. We dubbed this state Ψ^- as it is one of the four

2. Quantum state teleportation

so-called Bell states

$$\begin{aligned} |\Psi^-\rangle &= \frac{1}{\sqrt{2}}(|0\rangle|1\rangle - |1\rangle|0\rangle) \\ |\Psi^+\rangle &= \frac{1}{\sqrt{2}}(|0\rangle|1\rangle + |1\rangle|0\rangle) \\ |\Phi^-\rangle &= \frac{1}{\sqrt{2}}(|0\rangle|0\rangle - |1\rangle|1\rangle) \\ |\Phi^+\rangle &= \frac{1}{\sqrt{2}}(|0\rangle|0\rangle + |1\rangle|1\rangle). \end{aligned} \quad (2.5)$$

These states form a orthonormal base of the combined Hilbert-space of the two particles. All of them are maximally entangled states in the sense that a single particle of the pair carries no information on its own ². Only the relation between the two particles is well defined.

To teleport the state $|\chi\rangle_1 = \alpha|0\rangle_1 + \beta|1\rangle_1$ of particle 1, Alice has to perform a Bell state analysis (BSA) on this particle and her part of the shared entangled pair. That means, she has in principle to perform a measurement of an observable of the type

$$\hat{O}_{12} = \lambda_1|\Psi^-\rangle\langle\Psi^-| + \lambda_2|\Psi^+\rangle\langle\Psi^+| + \lambda_3|\Phi^-\rangle\langle\Phi^-| + \lambda_4|\Phi^+\rangle\langle\Phi^+|. \quad (2.6)$$

Here, the λ_i s stand for the corresponding eigenvalues of the observable, which are arbitrary values just to illustrate the distinction of the different Bell states in the measurement process. In the actual experimental realization of this measurement, the distinction of the Bell states bases upon the different distribution of detection events. This will be covered in section 3.2.1.

The Bell measurement projects the initially uncorrelated particles 1 and 2 on one of the four Bell states. Because of their initial independence, each of the four outcomes is equally probable. Due to the entanglement between particles 2 and 3, the projection of particles 1 and 2 on a well defined state will cause the state of particle 3 to become related to the original state of particle 1. Therefore, depending on the outcome of the measurement, particle 3 will be in one of the following states

outcome of BSA	state of particle 3
$ \Psi^-\rangle$	$-\alpha 0\rangle_3 - \beta 1\rangle_3 = U_1 \chi\rangle_3$
$ \Psi^+\rangle$	$-\alpha 0\rangle_3 + \beta 1\rangle_3 = U_2 \chi\rangle_3$
$ \Phi^-\rangle$	$\beta 0\rangle_3 + \alpha 1\rangle_3 = U_3 \chi\rangle_3$
$ \Phi^+\rangle$	$-\beta 0\rangle_3 + \alpha 1\rangle_3 = U_4 \chi\rangle_3$

As one can see, the state of particle 3 is correlated to the original state of particle 1 via a different unitary transformation depending on the outcome of the BSA. In the basis of $|0\rangle$ and $|1\rangle$ the four transformations and their inverses are:

²Of course this concerns only the degrees of freedom which are entangled.

outcome of BSA	U_i	U_i^{-1}
$ \Psi^-\rangle$	$\begin{pmatrix} -1 & 0 \\ 0 & -1 \end{pmatrix}$	$\begin{pmatrix} -1 & 0 \\ 0 & -1 \end{pmatrix}$
$ \Psi^+\rangle$	$\begin{pmatrix} -1 & 0 \\ 0 & 1 \end{pmatrix}$	$\begin{pmatrix} -1 & 0 \\ 0 & 1 \end{pmatrix}$
$ \Phi^-\rangle$	$\begin{pmatrix} 0 & 1 \\ 1 & 0 \end{pmatrix}$	$\begin{pmatrix} 0 & 1 \\ 1 & 0 \end{pmatrix}$
$ \Phi^+\rangle$	$\begin{pmatrix} 0 & -1 \\ 1 & 0 \end{pmatrix}$	$\begin{pmatrix} 0 & 1 \\ -1 & 0 \end{pmatrix}$

To finish the teleportation process Bob has to perform the according inverse operation on particle 3, e.g. U_2^{-1} if the outcome on Alice's side was $|\Psi^+\rangle$. In the case of outcome $|\Psi^-\rangle$ Bob has to do nothing as particle 3 will already be in the correct state.

For this last step Bob needs to know the outcome of Alice's BSA. This information can be encoded in 2 Bits and can then be sent to Bob via classical communication, as illustrated in figure 2.1.

It is important to note that, after the Bell state measurement, particle 1 is left with no information about its original state. Neither Alice nor Bob gain any information about the teleported state; it stays unknown and therefore it can be transferred to a different particle. If there was any gain of information, the transferred state would have to be in some way mutilated due to the no-cloning theorem.

3. Long distance quantum state teleportation

Since its proposal by Bennett et al [6] quantum state teleportation has been realized in several experiments, each taking a different approach. The scheme of D. Bouwmeester et al. [14] was the first to be realized and was nearest to the scheme proposed in Bennett et al.'s original paper, but it was refined to incomplete Bell measurements. The scheme of D. Boschi et al. [13] used only two particles instead of three (two entangled and one teleported) using entanglement of spatial modes. Additionally, the teleported photon was not independent but one of the entangled pair. Furusawa et al.'s scheme used continuous variables [24], while the first two schemes worked with finite dimensional variables (polarization in the first scheme, modes in the second). If quantum communication schemes using these continuous variables do really embody quantum effects or if they are just a very good classical simulation of these effects, is still under discussion[42].

The quantum states used in Bouwmeester's experiment and also in ours are the polarization states of single photons. Therefore, we realize a general qubit state $\alpha|0\rangle + \beta|1\rangle$ as the polarization state $\alpha|H\rangle + \beta|V\rangle$ of a single photon, where H represents horizontal and V vertical polarization. The advantages of using polarization are the following:

- it is easy to manipulate.
- the techniques for polarization manipulation are mostly linear optical devices and are highly sophisticated.
- up to now the most effective source of entanglement is parametric down-conversion (see subsection 3.2.2).
- in comparison to other degrees of freedoms like the excitation of ions, the lifetime of our states is very long and they are relatively stable against environmental noise. Therefore, the range for sending our states is incomparably larger than for any other carriers of quantum information (ions, etc.), which is crucial for any applications of quantum communication.

3.1. General Setup

Our group is now working on extending Bouwmeester et al.'s scheme (the Innsbruck scheme) to demonstrate teleportation over long distances at our

3. Long distance quantum state teleportation

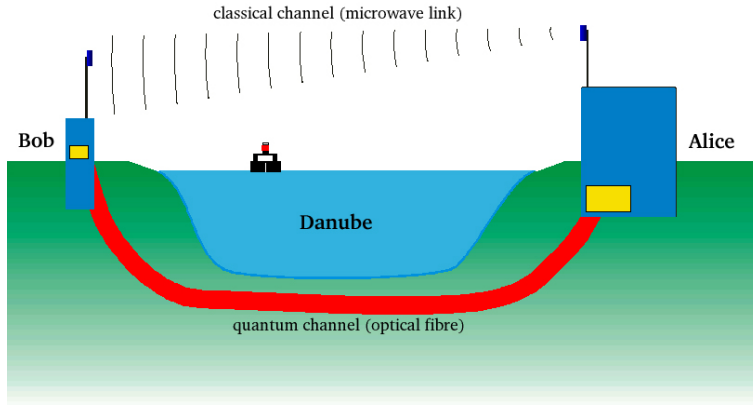


Figure 3.1.: (by Rupert Ursin) The scheme of the long distance quantum state teleportation project illustrates the buildings of the MA30 (a city magistrate providing us the facilities for our laboratories), the Danube in between them, separating our two parties Alice and Bob. They are connected via an optical fiber (the quantum channel) and a classical link (microwave transmitter and receiver).

Danube laboratories. These are situated at the facilities provided to us by the Magistratsabteilung 30 Wien-Kanal (shortly denoted as MA30)¹.

The distance between Alice's and Bob's laboratory along the beeline is approximately 580 meters, with the river Danube in between them. The channel for the entangled pair shared between them is a fiber of approximately 800 meters length, while the classical channel for sending Alice's measurement results has been realized by using a microwave broadcasting link (see section 3.3). See figure 3.1 for an illustration.

This teleportation experiment is planned to be the first to realize active switching. In all teleportation experiments up to now, Bob measured the state Alice teleported, without considering the information of Alice's Bell state measurement, as the teleported photon always arrived before the classical information. Subsequently, as up to now it is not reliably possible to store the state of photons to use them later on. Only those results could be taken into account for which Alice's BSA result was Ψ^- , as for all the other results Bob would have had to perform the according unitary transformation to regain the original state. In the Danube experiment the teleported photon is guided through an 800 m optical fiber. Thus, it is only propagating with $\frac{2}{3}c$, while the classical signal is broadcasted via microwave through air, thus propagating approximately with c .

Therefore, the classical signal will overtake the teleported photon and will reach Bob approximately $2 \mu s$ earlier. This is the time Bob will have to adjust a unitary transformation depending on Alice's outcome of the BSA.

¹The magistrate of Vienna responsible for the sewage network of the city.

The long distance teleportation setup can be coarsely parted in four sections:

- Alice's laboratory
- Bob's laboratory
- classical channel
- quantum channel

Alice's laboratory contains the entangled photon source and the BSA. First two entangled pairs are produced via spontaneous parametric down conversion (section 3.2.2). The first pair provides us on the one hand with a trigger photon and on the other hand with the photon we want to teleport. If we detect a trigger photon, we will know that our source has just produced some entangled pairs. That two pairs have been created, we ensure by always measuring fourfold coincidences; i.e. we count only those runs for which there are events at four detectors under consideration. For the teleportation scheme seven detectors are used. One as a trigger for the teleported photon, four for the more complete BSA and two for the polarization measurement on Bob's side. A successful fourfold coincidence comprises of an event at the trigger detector, an event at one of Bob's detectors and either a Ψ^- or a Ψ^+ coincidence at the BSA-detectors.

At the same time as the trigger photon is detected, the entanglement of this first pair is destroyed, but we do not need it anyway. All we need, is the knowledge that simultaneously the second particle of the pair is on its way: the photon to be teleported². This photon is sent through a polarizer for preparing the state we want to teleport.

Simultaneously, the second pair created provides the entanglement between Alice and Bob. One photon of the pair is sent to the Bell state analyzer together with the photon to be teleported. The second photon of the pair is sent to Bob via an optical fiber. The fiber runs through a tunnel below the Danube, called the Dük³, connecting Alice's and Bob's laboratories.

Subsequently, Alice performs a more complete Bell state measurement (see section 3.2.1). If her outcome is neither Ψ^- nor Ψ^+ , she will send nothing to Bob, so he won't even know about the "failure". If on the other hand it is one of the Ψ states, Alice will encode this information (subsection 3.3.4) and send it to Bob.

While for the Ψ^- outcome Bob does not have to perform any unitary operation on the arriving photon as it is already in the original state (see 2.2.2), for outcome Ψ^+ he has to perform a polarization-dependent phase flip given by the transformation

$$U = \begin{pmatrix} -1 & 0 \\ 0 & 1 \end{pmatrix}. \quad (3.1)$$

²In this way our source is a non-deterministic single photon source. If we detect a trigger photon, we will know for sure, that the associated second photon is on its way. Nevertheless, the source is undeterministic as it is impossible to predict, at which time a trigger photon is going to emerge.

³Dük^{er} is a german word meaning an underground crossing that bypasses some obstacle like a channel, a river, a street or a railway.

3. Long distance quantum state teleportation

When using polarized photons, this transformation can be realized by a half wave plate oriented in the computational basis (in our case vertically or horizontally). So, if Bob receives the message that Alice got outcome Ψ^+ , he will insert a half wave plate, while for outcome Ψ^- he will leave the teleported photon unchanged. In our specific experiment, Bob has about $2 \mu\text{s}$ time left to perform this operation.

Obviously, this cannot be managed by inserting a half wave plate mechanically or even by hand. An electro optical modulator (see chapter 4) has to be used to perform this task. In our case, a Pockels cell is used, which acts as a half-wave plate only if the correct voltage is applied to it (the $\lambda/2$ -voltage). Otherwise, the photon passes the Pockels cell unchanged. Therefore, all Bob has to do is either wait for the photon (in the Ψ^- case) or to switch his Pockels cell to the right voltage and then wait for the photon (Ψ^+ case).

When the photon arrives at Bob's side, it will enter the Pockels cell, which will by then be acting in the correct way and thus transform the photon such as to exactly resemble the original photon. This photon is then forwarded to a polarizing beamsplitter in the same basis as Alice coded the photon to check if the teleportation protocol has been successful (section 3.5).

In the following sections the four parts of the long distance teleportation setup will be covered one by one as listed above.

3.2. Alice's laboratory

Most of the setup on Alice's side is part of the source of entanglement, since although a lot of experimental and theoretical work has been done on entanglement and quantum information, it is still difficult and demanding work to actually create entangled particles. Up to now, the most efficient source of entangled photons is the process of *spontaneous parametric down conversion* (SPDC).

An overview over the whole setup in Alice's laboratory is given in fig. 3.2. As indicated, we will divide the setup in roughly three parts, the laser system used to pump the source, SPDC as our source of entanglement and at last the Bell state analysis. These three parts will be the topic of the following subsections.

3.2.1. Experimental Bell state analysis

As has been mentioned earlier (see ??), although a complete BSA is necessary for reliable nonpostselect teleportation, it is experimentally impossible to distinguish all four Bell states deterministically by using only linear optics⁴, as has been proven and discussed in several papers, see e.g. [46, 32, 17].

While a complete discrimination of the four Bell states is experimentally impossible, it is possible to experimentally perform an incomplete BSA. The first experimental scheme to do this was suggested by S. Braunstein and A. Mann

⁴Nevertheless, it is possible to distinguish all four states probabilistic, e.g. by using measurements as the necessary non-linear element. This way, one can succeed in determining any of the four states with a certain probability. For instance, one possibility would be to implement a probabilistic CNOT-gate.

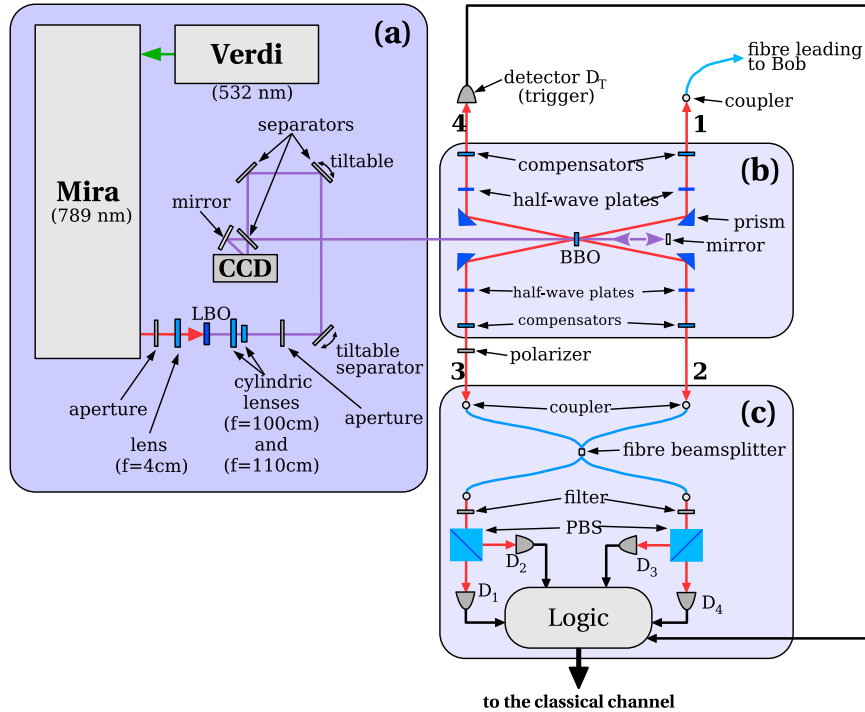


Figure 3.2.: For a clear description of Alice's laboratory we split it in three parts, indicated by the shaded squares. (a) represents the generation of our UV pump beam needed in our source (b) to generate the entangled pairs used in the teleportation scheme. In (c) the (more complete) BSA is performed and the result is sent on it's way to Bob. The four photons produced in the BBO are numbered from 1 to 4. Photons 1 and 2 build the pair providing the entanglement between Alice and Bob. Photon 3 indicates the photon to be teleported. An exact description of the setup will be given in the according subsections.

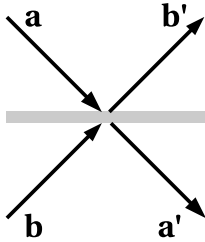


Figure 3.3.: A 50:50 symmetric beamsplitter regarded as an unitary transformation of its spatial modes.

[15]. Their scheme is based on the fact that the singlet state is antisymmetric while all other three Bell states are symmetric as will be explained in the following.

As photons are bosons, their wavefunction has to be symmetric with regard to exchanges of the particles. But as the spin part of the wavefunction of a singlet state is antisymmetric, the spatial wavefunction of the photons has to be antisymmetric, too, guaranteeing the symmetry of the combined wavefunction. For the other three Bell states, which are triplet states, the spin part of the wavefunction is symmetric with regard to the exchange of the particles and the same holds true for the spatial part.

With regard to the spatial modes of a beamsplitter (see fig. 3.3) the symmetric and antisymmetric spatial wavefunctions can be written as:

$$|a\rangle_1|b\rangle_2 \pm |b\rangle_1|a\rangle_2, \quad (3.2)$$

where the + stands for the symmetric, the - for the antisymmetric wavefunction. A 50:50 symmetric beamsplitter can be represented by the Hadamard transformation:

$$\frac{1}{\sqrt{2}} \begin{pmatrix} 1 & 1 \\ 1 & -1 \end{pmatrix}. \quad (3.3)$$

By applying a combined Hadamard transformation $H = H_1 \otimes H_2$ on the symmetric and the antisymmetric state⁵:

$$\begin{aligned} H(|a\rangle_1|b\rangle_2 + |b\rangle_1|a\rangle_2) &= |a'\rangle_1|a'\rangle_2 \pm |b'\rangle_1|b'\rangle_2 \\ H(|a\rangle_1|b\rangle_2 - |b\rangle_1|a\rangle_2) &= -(|a'\rangle_1|b'\rangle_2 - |b'\rangle_1|a'\rangle_2). \end{aligned} \quad (3.4)$$

Consequently, the antisymmetric state is an eigenstate of the Hadamard transformation while the symmetric state is not.

Therefore, if one brings the two particles of a Bell state to interfere on a 50:50 symmetric beamsplitter, the two photons of the singlet state will always take different outlets (fig. 3.5), while the photons of the three triplet states will always leave via the same outlet, see fig. 3.4. Generally, one could say that the photons of a singlet state at a beamsplitter behave like fermions, never going into the same state (in this case it is the spatial mode). The triplet state photons on the other hand behave like bosons, always sticking together.

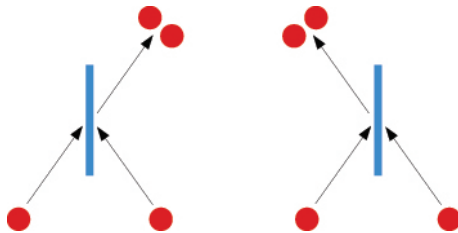


Figure 3.4.: When two identical bosons are brought to interfere at a 50:50 beamsplitter, they will interfere such that they always take the same outlet of the beamsplitter. The probabilities for the two cases (both exit left, both exit right) is 50% each.

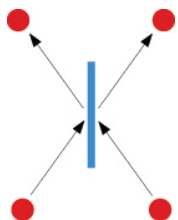


Figure 3.5.: The interference of two identical fermions at a 50:50 beamsplitter causes the two particles to leave certainly at different outlets. The probability for them leaving through the same outlet is naught.

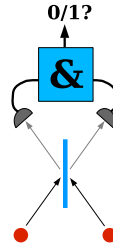


Figure 3.6.: If the two detectors register a coincidence (determined by the logical gate represented by the "&" -box), the incoming two particle state cannot have been bosonic. Therefore, the incoming state must have been Ψ^- , as it is the only Bell state not behaving bosonically. This scheme does not give us any information about the three other Bell states.

Therefore, if one of the four Bell states enters the beamsplitter we will afterwards get a coincidence in our two detectors at the outlets (see fig. 3.6) if and only if it was a singlet state. Also, if we let two photons being in any arbitrary state interfere on a 50:50 beamsplitter, a coincidence measurement will project them in a ψ^- -state.

This is the easiest type of a Bell state measurement, only distinguishing between ψ^- and the rest (a mixture of the other three Bell states).

In 1996 this technique was drastically improved by inserting an additional measurement after the beamsplitter [33]. In each path leaving the beamsplitter, a polarizing beamsplitter is placed (see fig. 3.7). Now we have four detectors and depending in which combination they fire, we will know if the measured state was a $|\Psi^-\rangle$, a $|\Psi^+\rangle$ or one of the Φ -states (or simply noise). The discrimination works as follows:

Detectors clicking	state measured
$(D_1 \wedge D_3) \vee (D_2 \wedge D_4)$	$ \Psi^-\rangle$
$(D_1 \wedge D_2) \vee (D_3 \wedge D_4)$	$ \Psi^+\rangle$

The discrimination between these two cases is done by a programmable logic. This logic produces a TTL signal on one of two BNC outputs, depending on the combination of detectors firing. If neither combination of detectors is met (e.g. only D_3 fires), the logic will not give any pulse. Therefore, two coaxial cables are leading to the classical channel, one carrying a TTL pulse if the logic detected a Ψ^- state, the other carrying a TTL pulse, if it was a Ψ^+ . This information, carried by the two cables, is later on combined into one signal by amplitude coding (see subsection 3.3.4).

⁵Here H_1 and H_2 stand for Hadamard transformations on particles 1 and 2.

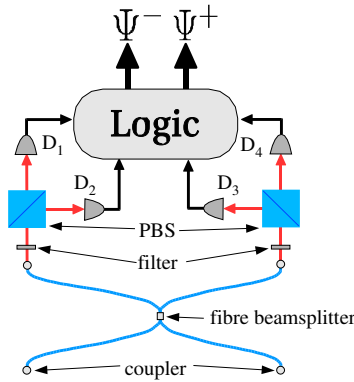


Figure 3.7.: A more complete Bell state analyzer discriminates three outcomes. Ψ^- will give us one click left and one click right. For Ψ^+ both photons go either left or right but they are splitted at one of the PBS. Therefore, we will get a coincidence either of the two detectors on the left side or of the two detectors on the right side. For any Φ -state, on both sides one detector will click.

3.2.2. Theory of SPDC

SPDC is a nonlinear effect appearing only in non-centrosymmetric crystals⁶, which can be seen as the decay of a pump photon in two *down converted* photons customarily called signal and idler⁷. As in every particle decay, energy and momentum must be conserved. However, since this picture is only an approximation, the conservation laws, too, hold only approximately:

$$\omega_p \cong \omega_s + \omega_i \quad (3.5)$$

$$\vec{k}_p \cong \vec{k}_s + \vec{k}_i. \quad (3.6)$$

Here, index p denotes the pump photon, s the signal photon, and i the idler photon. Additionally, signal and idler photon are highly time-correlated; i.e. if their optical paths from the source to the detector are equal then also their detection times will be equal up to the resolution of the detection system.

In general, there are two types of SPDC, depending on the polarizations of the photons created. Type I downconversion denotes the case where both photons have the same polarization, whereas Type II downconversion denotes the case where the two polarizations are orthogonal to each other.

To derive the phase matching conditions given above, we start with a semi-classical ansatz and derive the quantum mechanical limit (to be exact: the QED-limit) for single photons.

⁶In centrosymmetric crystals the term responsible for SPDC vanishes.

⁷This process has first been experimentally investigated by Burnham and Weinberg [16].

Entanglement between the created pairs of particles has first been experimentally demonstrated by Alley and Shih [1]. Ou and Mandel [35, 36] then triggered the extensive work on entanglement created via SPDC through their numerous fundamental experiments. In 1995 Kwiat et al. introduced the type of SPDC setup we are using today[30].

3. Long distance quantum state teleportation

If one assumes that the interaction between the electric field $\vec{E}(\vec{x}, t)$ and the polarization $\vec{p}(\vec{x}, t)$ takes place only at \vec{x} , the polarization evoked by the electromagnetic field can be written expanded in the Taylor series

$$p_i(\vec{x}, t) = \sum_{j=1}^3 \chi^{(1)}(\vec{x})_{ij} E_j(\vec{x}, t) + \sum_{j,k=1}^3 \chi^{(2)}_{ijk}(\vec{x}) E_j(\vec{x}, t) E_k(\vec{x}, t) + \dots, \quad (3.7)$$

where E_i describes the electric field in the crystal, $\chi^{(1)}$ and $\chi^{(2)}$ are the linear and second order polarizability coefficients. Now, $p_i(\vec{x}, t)$ gives us the polarization of a small volume δV around \vec{x} , which on the other hand consists of still smaller discrete quantities like atoms, ions or molecules⁸ carrying an electric dipole moment:

$$p_i(\vec{x}) \propto \sum_n \mu_n(\vec{x}) \delta(\vec{x} - \vec{x}_n), \quad (3.8)$$

with the sum extending over all atoms contained in the volume, V , of the crystal that is subject to the electromagnetic field of the pump.

As the interaction energy of an electric dipole $\vec{\mu}$ with the electric field is proportional to $\vec{E} \cdot \vec{\mu}$, the complete interaction Hamiltonian of the process will be proportional to

$$H_{int} \propto \int_V d^3x \vec{p}(\vec{x}, t) \vec{E}(\vec{x}, t). \quad (3.9)$$

The electric field \vec{E} can now be written as a superposition of \vec{E}^{pump} , the field of the pump, and \vec{E}_q , the second order field:

$$\vec{E}(\vec{x}, t) = \vec{E}^{pump}(\vec{x}, t) + \vec{E}^q(\vec{x}, t). \quad (3.10)$$

Now, if we quantize the electric fields, in the Schrödinger picture we get

$$\begin{aligned} \vec{E}(\vec{x}, t) &= \sum_{p=1}^2 \int d^3k \frac{i\sqrt{\omega}}{\sqrt{2\omega(2\pi)^3}} \hat{e}(\vec{k}, p) a(\vec{k}, p) e^{i(\vec{k}\vec{x} - \omega t)} + h.c. \\ &= \vec{E}^{(+)}(\vec{x}, t) + \vec{E}^{(-)}(\vec{x}, t), \end{aligned} \quad (3.11)$$

where $\hat{e}(\vec{k}, p)$ denotes the unit basis vectors (index p) of the polarization of a photon with wave-vector \vec{k} . After the quantization, each term \vec{E} will contain two terms, one with a creation operator $a^\dagger(\omega)$ (denoted as $\vec{E}^{(-)}$) and one with the annihilation operator $a(\omega)$ (denoted as $\vec{E}^{(+)}$) of the according frequency. Therefore, if we insert equ. (3.11) in equ. (3.7) and the result in equ. (3.9), two terms of interest for us will appear. One will contain a product $a^\dagger(2\omega)a(\omega)a(\omega)$ and another will contain the associated hermitian conjugate $a(2\omega)a^\dagger(\omega)a^\dagger(\omega)$. The first term is corresponding to the well known phenomenon of second harmonics generation, while the second term is the one responsible for SPDC. This is, of course, the term, we will concentrate on and so we get for the SPDC part of the interaction Hamiltonian

$$H_{SPDC} \propto \int_V d^3x \chi_{ijk} E_i^{pump} E_j^{(-)} E_k^{(-)}, \quad (3.12)$$

⁸In the following we will shortly denote these discrete quantities as "atoms".

where the pump field shall be

$$\vec{E}_{pump}(\vec{x}, t) = \vec{E}_p e^{i(\vec{k}_0 \vec{x} - \omega_0 t)} + h.c. \quad (3.13)$$

We have chosen a classical description of the pump field, which is valid as it has to be of very high power for the effect being noteworthy.

Inserting the quantized expressions for the electric fields into (3.12), we get several terms containing \vec{x} . If we collect these terms and integrate separately over them, we get

$$\int_V d^3x e^{i\vec{x}(\pm\vec{k}_p - \vec{k}_s - \vec{k}_i)}, \quad (3.14)$$

which approaches the delta-function $\delta(\pm\vec{k}_p - \vec{k}_s - \vec{k}_i)$ for large illuminated volumes V . The interaction Hamiltonian will, therefore, be only nonvanishing for argument of the delta-function being zero.

If one performs a similar calculation for the Hamiltonian of the process in the Dirac interaction picture⁹, one will arrive at a similar integral over the interaction-time of the pump-field with the crystal:

$$\int_{-\frac{L}{2c}}^{\frac{L}{2c}} dt e^{it(\pm\omega_p - \omega_s - \omega_i)}, \quad (3.15)$$

where we have assumed that the crystal is cubic with L the length of its edges. For long interaction times (L large) this is again approximately a delta-function. From the condition that there are no negative frequencies, it follows that we have to choose the plus sign in both of the above delta-functions; i.e. the interaction Hamiltonian is proportional to $\delta(\vec{k}_0 - \vec{k}_s - \vec{k}_i)$ and $\delta(\omega_0 - \omega_s - \omega_i)$. Therefore, SPDC produces only photons fulfilling the phase matching conditions (3.6) and (3.5). As mentioned before, these conditions are only approximately fulfilled, as the size of the crystal is finite. Nevertheless, as the dimensions of the crystal are several magnitudes larger than the wavelengths of the pump and the down converted photons, the approximation is in general very accurate.

3.2.3. Experimental setup of SPDC as entanglement source

As we have seen in subsection 3.2.2, SPDC is a nonlinear effect occurring in crystals when pumped by a high intensity coherent light source. The efficiency of the process is thus determined by the nonlinear coefficients of the crystal. For this reason a BBO crystal¹⁰ is used, due to its high nonlinear coefficient $\chi^{(2)}$ responsible for SPDC. It is cut in such a way that in the case of degenerate wavelengths ($\lambda_s = \lambda_i$) the downconverted photons are non-collinear ($|\vec{k}_s \cdot \vec{k}_i| < |k_{signal}| \cdot |k_{idler}|$). Figure 3.8 shows a scheme of the process for the frequency-degenerate case. According to the phase matching condition in equation (3.6), the downconverted photons emerge from the BBO on cones. One cone for the extraordinary beam (vertically polarized) and one for the ordinary

⁹This must be done to obtain the time evolution of the resulting fields.

¹⁰BBO stands for β -BaB₂O₄.

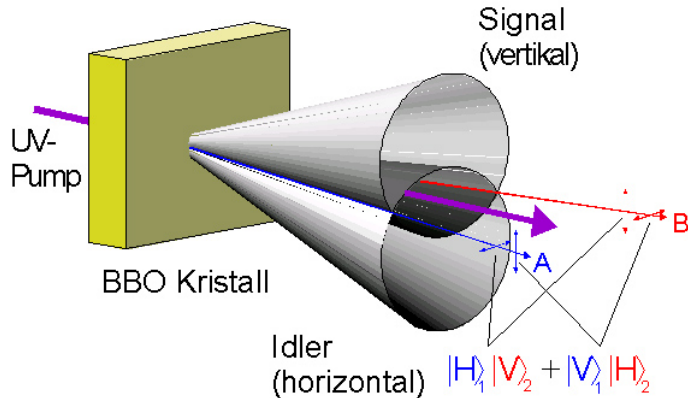


Figure 3.8.: Via the process of spontaneous parametric downconversion in an anisotropic crystal (BBO), one photon of the UV laser pump decays in two photons under approximate conservation of energy and momentum. In type II downconversion, which is illustrated here, one photon is horizontally polarized, the other one vertically. Therefore, they are passing the birefringent crystal along different ways. In the case where the photons have the same frequency, they leave the crystal along the vertices of the two cones (one for the ordinary, one for the extraordinary beam). Along these lines, we do not know which photon comes from the upper and which one from the lower cone. Therefore, we do not know, if the right one is horizontally polarized and the left one vertically or if it is the other way round. Hence, we get an polarization entangled state as indicated.

beam (horizontally polarized). In his PhD-thesis, G. Weihs[48] performed calculations based upon the phase matching conditions (3.5) and (3.6) and the crystal parameters determining the properties of the downconverted photons in dependence of the relative orientation of the pump beam to the optical axis of the crystal. He found that the optimal orientation of the crystal relative to the pump beam is such, that the intersection lines of the ordinary and extraordinary cone enclose an angle of approximately 6° ; i.e. the angle between the intersection lines and the pump beam is 3° .

In order to create two entangled pairs, the pump beam passes the BBO twice (see fig. 3.9). Therefore, the second pair is created a time $t = 2d/c$ later than the first one, where d is the distance between the BBO and the mirror on which the pump beam is reflected.

To allow interference between two photons of different pairs on a beamsplitter (for the BSA), the photons have to be indistinguishable. This means that either they have to overlap on the beamsplitter within their coherence time, T_c , or the information about the arrival time of the photons has to be erased (quantum eraser). In our experiment we choose the first possibility and therefore it is necessary that $t < T_c$, resulting in:

$$d < c \cdot T_c / 2. \quad (3.16)$$

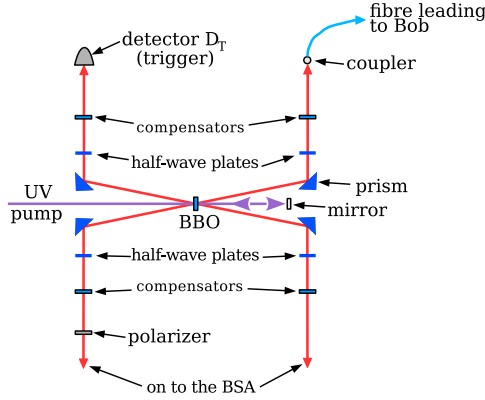


Figure 3.9.: To achieve spontaneous parametric downconversion, a BBO crystal is pumped by a pulsed high intensity UV laser. The pump beam passes the BBO two times, creating two photon pairs. As we are dealing with type II down conversion, we have to compensate for the longitudinal walk off between the two photons which occurs due to their different polarization while passing through the BBO, as otherwise the photons would be distinguishable in principle by their arrival times at the detectors. Additionally, the polarizer for preparing the teleportation state and the fiber leading to Bob's laboratory are shown.

This dependency of the interference visibility at the beamsplitter of the distance between mirror and BBO can be visualized by plotting the probability for a coincidence measurement at the two outlets of the 50:50 beamsplitter of the BSA over the position of the mirror. At the point where the lengths of their paths from their creation to the beamsplitter are the same for both photons, there should be no coincidence counts, as they are indistinguishable in this case and therefore take always the same output mode (bosonic behavior). The farther the mirror gets from this optimal position the more the photons become distinguishable. If they are totally distinguishable, the probability of a coincidence count will be 1/2; i.e. the curve will be constantly 1/2 most of the way and ideally decreasing to zero in the vicinity of the point, where the path lengths for the photons are equal. This dip in the photon distribution is called Hong-Ou-Mandel dip [25].

As any stable alignment gets more difficult with the distance, it is generally a good idea to keep the size of the down conversion setup as small as possible. Additionally, this leaves more space for other parts of the experimental setup and it allows for a higher coupling efficiency. But as the angle between the pump and the downconverted photons is only about 3°, the space between the two beams of downconverted photons is rather limited and it would need about one meter distance until the space between the two beams would be sufficient to place two couplers next to each other. To circumvent these long distances, we

3. Long distance quantum state teleportation

deflects the down converted photons by mirror coated prisms in the direction of the according couplers (see fig. 3.9).

Those photons created in the BBO, which have the correct frequency (frequency degenerated case) are selected geometrically; i.e. we place single mode optical fibers such that approximately only the photons coming along the vertices of the cones shown in picture 3.8 are coupled in. The use of single-mode fibers allows at the same time further discrimination of the background signal due to their spatial mode selectivity [29].

Due to the birefringence of the BBO, the horizontally polarized photon and the vertically polarized one will pass through it with different velocities. Therefore, there will be a time delay between them, when they emerge from the crystal - an effect known as longitudinal walk-off. This delay, however, could be measured and thus be used for discriminating between horizontally and vertically polarized photons. To get entanglement between the two photons, this possibility must be prevented.

In principle, this can be done by sending each downconverted photon through another BBO. If the optical axis of this second BBO is perpendicular to the first one's, the photon which was the faster one in the first BBO will now be the slower one and the other way round. As parametric down conversion is a spontaneous effect, the probability for the pump photon to decay in two down converted photons is equal at each point of its way through the crystal. Therefore, the down converted photon can origin from any point along the path of the pump photon and thus the magnitude of the longitudinal walkoff is random. If the down-converted photons are generated shortly after the pump photon enters the crystal, the walk-off will be largest. The farther the pump photon moves through the crystal before it decays, the smaller gets the walkoff and it vanishes if the photons are created just at the end of the pump photon's way through the crystal. If we send the photons through a compensator, the leading photon will be delayed. Hence, the information, which polarization corresponds to the particle arriving first is destroyed in average (see fig. 3.10).

Instead of orienting the optical axis perpendicular to the BBO's optical axis, we orient the optical axis of the compensators parallel to the BBO's and put halfwave-plates between compensators and BBO. This has theoretically the same effect as orienting the axis orthogonal to each other. Experiments showed, however, that the method using halfwave plates, leads to a much higher visibility. Probably, this depends on how the crystals are cut.

Additionally, other walk-off effects occur during SPDC, namely the transversal and the spectral walk-off. Due to birefringence the ordinary and extraordinary beam propagate along different directions inside the crystal although they become collinear again outside the crystal. This transversal walk-off, however, is also compensated by the crystals used to compensate the longitudinal walk-off.

The spectral walk-off, on the other hand, is not compensated for in our experiment. It is an effect only occurring when pumping the BBO with a pulsed laser. The broader the bandwidth of the pump pulse gets, the more the spectra of the extraordinary and the ordinary photons differ from each other. Therefore, the two photons get more and more discriminable resulting in a lower

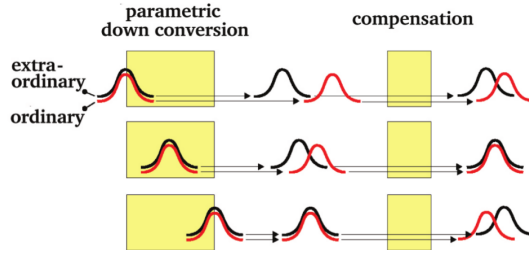


Figure 3.10.: As the parametric down conversion is a spontaneous process, the decay of the pump photon in the two down converted photons can happen at any point in the crystal. Therefore, the delay between a horizontally and a vertically polarized photon varies between zero and the maximum value depending on the thickness of the BBO. By inserting compensators, one can delay the first photon to blur the information, which of the two photons is first.

visibility of the entanglement.

3.2.4. The laser system pumping the BBO

As mentioned earlier, the BSA performed by Alice on the photon to be teleported and on one photon of the shared entangled pair, is based upon the interference of these two photons at a 50:50 beamsplitter. In the last subsection, we saw that the difference in the paths of the photons from their creation to the beamsplitter have to be nearly equal (within their coherence length) to allow interference. This implies, however, that the time of their creation is well known.

Therefore, as the two photons originate from two different entangled pairs, the variations in the delay between their creation times must be shorter than their coherence time. Since SPDC is a spontaneous effect and can occur at any time during which the crystal is pumped by the laser, the time interval in which the creation of an entangled pair takes place, can only be limited by a finite interaction time of the laser with the crystal. This can in principle either be done by taking a very thin crystal or by pulsing the pump laser. It turns out, however, that the first method is not feasible as it would need the crystal to be only several microns thick, but this would result in very low count rates and inaccurate phase matching conditions. If we use a pumped laser, pair creation will only occur during the times a pulse passes through the crystal. That means, the shorter our laser pulses get, the better we know the time delay between the creation of the two pairs. Unfortunately, the coherence time of the photons gets simultaneously shorter. Hence, the optimal solution has to be somewhere in between too long and too short pulses in order to allow for a good visibility of the interference at the beamsplitter.

A pulse width of approximately 200 fs proved to be optimal for this purpose, which is not too hard to realize. To generate 100 fs pulse-widths is a standard procedure these days using mode-locked lasers in the near infrared. The system

3. Long distance quantum state teleportation

we use is a Mira900aBasic (Ti:Sapphire laser, 789 nm, 150 ns pulses), pumped by a 10 W Verdi, which is a 532 nm solid state laser. The average power output of the Mira is around 1.3 W, where the interval between two pulses is approximately 13 ns (equivalent to a repetition rate of ~ 76 MHz). An operating wavelength of 789 nm has been chosen mainly because of the relatively high single photon detection efficiencies at this wavelength.

Now, to get 789 nm downconverted photons out of the BBO, it has to be pumped by light of the half wavelength. Therefore, we have to upconvert the pump before using it for downconversion. For this purpose, the pump beam is focused on a LBO-crystal (lithium borate), cut for type-I second harmonic generation, the counterpart to parametric downconversion. On the particle level, the process can be described as the creation of one ultraviolet photon out of two infrared photons, with a typical efficiency of 25%-30% [28]. Thus, about 400 mW of 394.5 nm ultraviolet light are generated.

The beam profile of the emerging light is elliptical due to the birefringence of the LBO crystal. We compensate this effect using two crossed cylindrical lenses (UV grade silica glass)[28]. Now we are left with the ultraviolet laser pump we need for parametric downconversion. Figure 3.11 shows the overall setup for the generation of the pump beam.

Since the setup is very sensible to any change in the alignment of the pump beam, it is necessary to compensate any walk offs the beam could suffer over time. For this purpose Th. Jennewein designed a computer program noticing any walk off of the beam and compensating it by automatic new alignment of motorized mirrors in the setup [28]. For this purpose some UV-light leaking through dichroic mirrors¹¹ was recorded by a CCD-camera (see fig. 3.11). The pictures taken contain two spots of UV-light, one of the beam before passing the BBO, the second of the beam after it has gone through the BBO. The picture taken, is then processed by a Labview program, which has been fed by reference positions taken at a time when the setup was well aligned. Therefore, the program only has to move the motorized mirrors until the current laser spots coincide with the reference positions.

3.3. The classical channel

The classical channel should allow a safe and constantly timed transmission of the classical information necessary to perform teleportation. Safe means in this context, that any signal we send over the channel should arrive recognizably at Bob's side. "Constantly timed" means that the delay between a teleported photon and the corresponding classical signal should be either constant over time or at least predictable with sufficient accuracy. Additionally, the total time necessary for processing the signal on both, the sender and the receiver side, should be not larger than $\sim 2 \mu\text{s}$ at most¹², as it has to be finished before

¹¹This type of mirrors consists of dielectric layers, such that the UV light generated in the LBO is nearly perfectly reflected, while the spare infrared light is transmitted and can be used for alignment purposes.

¹²The time Alice's classical signal arrives earlier at Bob's side than the teleported photon.

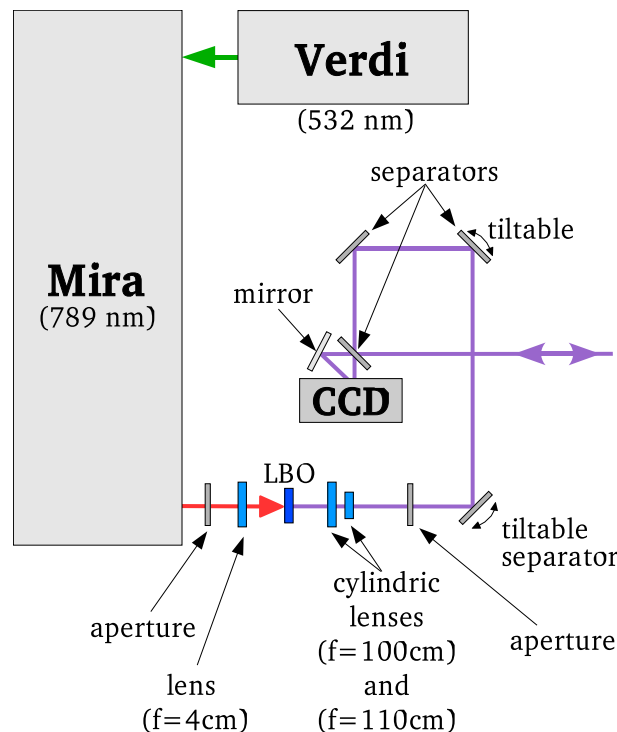


Figure 3.11.: Our ultraviolet pump beam is created via second-harmonics generation in an LBO crystal, which is pumped by a mode-locked Mira, which again is pumped by a Verdi laser. While the 4 cm lens after the Mira is just for focusing the beam on the LBO, the cylinder lenses are needed to give the resulting ultraviolet beam an approximately Gaussian profile. To ensure the stability of the pump beam position, those small parts of the UV light which are not reflected by the separators (dichroic mirrors) are monitored with a CCD. A computer checks the position of the pump beam by interpreting the CCD pictures and moves the two tiltable mirrors in order to correct any spatial drifts.

3. Long distance quantum state teleportation

the teleported photon arrives. This rules out any computer use in the processing of the signal, however fast it is coded. The only way to meet these requirements is to process the signal electronically using high frequency circuits. Thus, we use video link equipment adopted for sending and receiving high frequency signals.

3.3.1. Transmitter and receiver

We use a microwave link operating at an adjustable frequency in the 2.4 GHz Industrial, scientific and medical (ISM) band. ISM-bands are frequency bands free to the public for non-licensed use. The band we use reaches from 2.4000 GHz to 2.4835 GHz. Since these bands are free, they find a variety of different uses; the link we use, for instance, is usually used for the signals of outdoor security cameras. The transmitter and receiver units encode their signals via Fourier transformation. This means, if we send a binary signal coded by choosing some amplitude for the signal, this pulse will not be directly transmitted but will be encoded via frequency modulation (FM). This has some great advantages over sending the signal directly via amplitude modulation:

1. improved signal to noise ratio
2. smaller geographical interference between neighboring stations¹³
3. less radiated power
4. well defined service areas for given transmitter power

But there are also disadvantages of using such a link. One is that the bandwidth needed for transmitting frequency modulated signals is larger by far than in the case of amplitude modulation, and the transmitter and receiver units are technically more complex. Additionally, the signals produced by the coincidence logic are too long (~ 200 ns) to be accurately encoded with the transmitter and receiver bandwidths (30 Hz to 5 MHz). Furthermore, the coaxial cables used in connection with these units all have a resistance of 75Ω , while all other coaxial cables used in our setup have a resistance of 50Ω . Therefore, a kind of translator has to be used to ensure an operating communication between our devices and the microwave link (see section 3.3.4).

Both the sender and receiver possess five channels working at different frequencies. Therefore, we had the possibility to choose between them in order to find the best possible link. This was made necessary by our use of other microwave based antennas used for a wireless internet connection between Alice's and Bob's laboratory we used to control devices at Bob's side and to read out Bob's data. These antennas too possessed different freely choosable channels for transmission and so we tested several combinations until both links were working optimally.

For the exact specifications of the microwave link see appendix A.2.

¹³This is because in FM signals the amplitude bears no signal information. Therefore, the amplitude can be used to obtain some additional information. For instance, the receiver of a signal can easily determine the signal of the nearest sender by choosing the one with the largest amplitude. In AM signals the information is coded in the amplitude, thus making it difficult to determine the nearest sender.

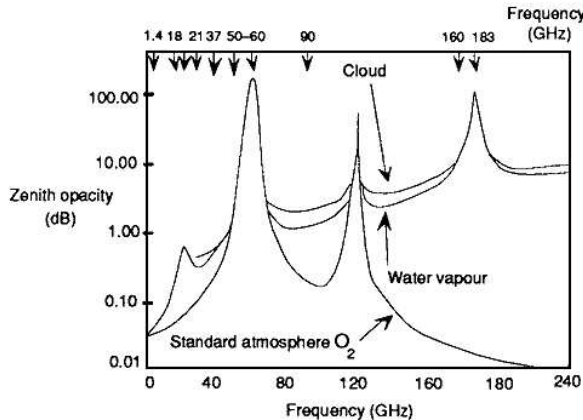


Figure 3.12.: Atmospheric microwave absorption. Strong absorption features appear as peaks. The three curves show absorption in a dry atmosphere, in the same atmosphere with 20 kg/m^2 of added water vapor, and with both water vapor and 0.2 kg/m^2 of stratus cloud added. Valleys are microwave windows. From Murphy et al. (1987)[40].

3.3.2. Link stability

As lined out in the beginning of this section, the demands we make on the classical channel are rather strict. Therefore, its stability is an important point to consider and makes it necessary to reflect upon possible distortions of the signals or even breakdowns of the radio link.

As microwave ovens work at 2.45 GHz it is tempting to think that this frequency lies near a resonance of water. Nevertheless, there is nothing special about this frequency. It was only chosen for the operation of microwave ovens because it lies in the ISM band and is therefore free for industrial use [8]. The attenuation of microwaves due to liquid water in the atmosphere gets really noteworthy from 10 GHz on and the attenuation due to water vapor becomes interesting around 20 GHz (see fig. 3.12).

Nevertheless, there will of course be some attenuation at normal weather conditions and the distortions might even get drastic for heavy falling rain, although there have not been scans yet on rainy days. Fact is however, that trees in the line of transmission seriously effect the link operation, leading to heavy distortions of the signals or even total breakdowns of the link.

Effects of this kind, probably due to trees, were observed when trying to measure the delay between the classical link and the fiber link between Alice and Bob.

3.3.3. The delay between classical and quantum channel

Since the teleported photon travels only at two thirds of the velocity of light while propagating through the fiber between Alice and Bob (the "quantum channel"), the according classical signal will overtake the photon as it travels through air at nearly the full velocity of light. However, the exact velocity of the classical signal depends on the refractive index of air for the wavelength used. The question to be answered here, is whether natural influences will lead to noticeable fluctuations (> 10 ns) in the classical signal propagation speed.

The refractive index of air depends on the typical parameters of a gas. These are the concentration of its constituents, their temperatures and their partial pressures. In general the distributions of these parameters will vary over space and time and, as it would require an exact knowledge about the state of the atmosphere, an exact calculation of the refractive index of air is impossible. So, all predictions of the refractive index must base on simplified models. The accuracy of these models however is quite good, and thus we will choose the simplest model meeting our demands of accuracy.

As indicated in section 4.5.2¹⁴, the width of the coincidence window used on Bob's side is about 30 nanoseconds. Any changes of the delay due to changing weather conditions should therefore fulfill:

$$\Delta t_{path} < 30\text{ns}. \quad (3.17)$$

As the distance between Alice and Bob is ~ 580 m, the time for the signal to pass it is $t_{path} \simeq 580/c_a$, where $c_a = n_a c$ is the velocity of light in air with the refractive index n_a . Therefore, we get

$$\Delta t_{path} \simeq \frac{580}{c_a^2} \Delta c_a = \frac{580}{cn_a^2} \Delta n_a \simeq \frac{580}{c} \Delta n_a < 30\text{ ns}, \quad (3.18)$$

where we assumed n_a^2 to be approximately 1. From this we get an upper bound for the tolerable error of n_a :

$$\Delta n_a < 1.56 \times 10^{-2}. \quad (3.19)$$

Now, we can check if changes of the weather conditions would lead to a change in the refractive index surpassing the tolerable error. We will do that by using an empiric formula based upon the 1951 paper of Essen and Froome [22]

$$(n_a - 1) \times 10^6 = \frac{77.6}{T} (p - e) + e \frac{64.8}{T} + 3.776 \times 10^5 \frac{e}{T^2}, \quad (3.20)$$

where the numerical coefficients were experimentally determined in 1974 by G. Thayer [45]. Here, T is the temperature (K), p is the air-pressure (hPa), and e is the water-vapor pressure (hPa). The first term on the right side of the equation can be seen as the "dry" part of the refractive index, while the second and third term can be seen as the wet part due to air humidity. In addition,

¹⁴In "The delay between classical and quantum channel".

Thayer introduced corrections for nonideal gases to the formula above. With these corrections, the formula reads

$$(n_a - 1) \times 10^6 = \frac{77.6}{T}(p - e)Z_a^{-1} + e\frac{64.8}{T}Z_w^{-1} + 3.776 \times 10^5 \frac{e}{T^2}Z_w^{-1}, \quad (3.21)$$

where the correction factors Z_a and Z_w are given by[37, 45]

$$\begin{aligned} Z_a^{-1} &= 1 + (p - e)[57.9 \times 10^{-8}(1 + 0.52/T) - \\ &\quad 9.4611 \times 10^{-4}(T - 273.15)/T^2] \\ Z_w^{-1} &= 1 + 1650(e/T^3)[1 - 0.01317(T - 275.15) + \\ &\quad 1.75 \times 10^{-4}(T - 273.15)^2 + 1.44 \times 10^{-6}(T - 273.15)^3]. \end{aligned} \quad (3.22)$$

To check whether common changes in temperature, pressure or humidity affect the refractive index in a way noticeable in our signal velocity, we will vary the parameters in equation (3.21) within the limits listed in the following table:

parameter	minimum value	maximum value
p	970 mb	1050 mb
T	258 K	310 K
U	0%	100%

The limits given here are rather extreme in order to get a broad bandwidth of possible changes to the refractive index. For instance would it need a full-grown storm to get an air pressure as low as 970 mb. In the above table, we introduced the humidity of air. It is given by

$$U = 100 \cdot \frac{e}{e_S(T)}, \quad (3.23)$$

where $e_S(T)$ is the saturation vapor pressure, which can be calculated using Magnus' formula:

$$e_S(T) = 6.1078 \cdot \exp\left(\frac{17.27(T - 273.15)}{T - 35.85}\right). \quad (3.24)$$

To estimate the maximum change in refractive indices to be expected by changing weather conditions, we ought to have normal weather conditions as a reference. As we will compare these reference conditions to quite extreme weather conditions, the reference is nearly arbitrary. Therefore, we just took the conditions measured in Vienna on the day this was written:¹⁵, $p_{now} \simeq 1030 \text{ mb}$, $T_{now} \simeq 278 \text{ K}$ and $U_{now} \simeq 70\%$. As p enters linearly into the refractive index of air, it is enough to consider the different refractive indices for the two extreme values of pressure (970 and 1050 mb). Anything in between would surely differ less from our reference values. The difference between the refractive index at our reference conditions and at a constant air pressure of 1050 mb and varying temperature and humidity is plotted in fig. 3.13. For an air pressure of 970 mb the same is plotted in fig. 3.14. From the graphs it is obvious that the maximum

¹⁵That is, the 16th of January, 2003.

3. Long distance quantum state teleportation

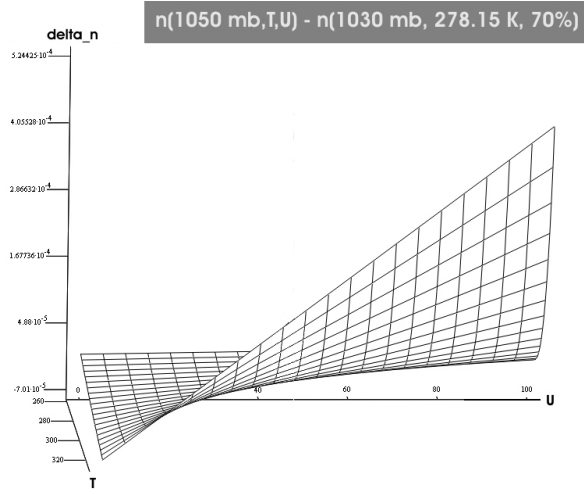


Figure 3.13.: The difference in the refractive index between normal conditions (1030 mb, 5°C, 70% humidity) and conditions at 1050 mb and varying temperature and humidity.

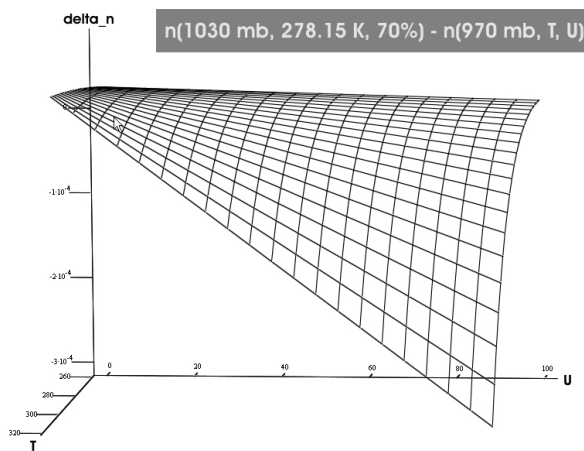


Figure 3.14.: The difference in the refractive index between normal conditions (1030 mb, 5°C, 70% humidity) and conditions at 970 mb and varying temperature and humidity.

change relative to normal conditions and even of the two extreme functions relative to each other reaches maximally $\Delta n \simeq 5 \times 10^{-4}$, and even this only in the case of temperatures never occurring in Vienna, like 45°C combined with 100% humidity. Therefore, the usual changes in our delay due to changing weather conditions are below one nanosecond and thus well below the limit of 30 ns we considered above.

Considering that, we see that changes of the weather conditions will not lead to any noteworthy effect on the velocity of the microwave signals. Scans of the traveling time of the signals plotted over time should therefore remain constant up to one nanosecond as long as there are no additional yet unknown effects on the measured traveling time other than the change of the refractive index. For instance it is possible that the electronic devices used for signal processing operate more slowly or less accurate under varying conditions. Especially, the humidity could affect the circuits in a negative way. Such effects are not considered in the calculations and should thus be noticeable in the scans.

Scans of the delay between classical and quantum signal

To verify the stability of the classical channel (i.e. the timing stability between classical and quantum channel), we performed several scans of the delay of the quantum relative to the classical signal over times on the scale of the duration of an actual teleportation-scan (about 18 hours).

The easiest way to get a good approximation of the stability of the time delay between signals passing via the classical channel and signals passing via the optical fiber (the quantum channel), is to generate a TTL pulse and send it simultaneously via the classical channel and via a coaxial cable taking the same way as the optical fiber. The coaxial cables are used because it is simple to measure the time delay between two equivalent electronic signals. Although the time delay measured is in good approximation equal to the one between classical channel and fiber¹⁶, we are only interested in changes of the time delay. Therefore, the velocity of the reference signal is not of relevance.

If the measurement devices are treated as not changing their processing speed under varying weather conditions, the delay between the two signals will only depend on the difference in their velocity. Since the fiber and the coaxial cable are run in a tunnel well below ground level, the climate conditions of their surroundings can be treated as stable and therefore the velocity of the signal in the coaxial cable will be constant. Hence, any change in the delay must be due to changes in the velocity of the classical signal and thus due to changes of the refractive index. Taking this point of view we would expect variations in the time delay of maximally 1 ns.

An according measurement has been performed by sending TTL signals produced by a function generator simultaneously through the cable and via the microwave link from Alice to Bob. In Bob's laboratory the delay between the two signals was measured by an SR620 counter. The frequencies of the different delays are plotted in fig. 3.15 fitted by a Gaussian. According to the data taken

¹⁶According to the manufacturer the propagation velocity of signals in the coaxial cables is 66% of the velocity of light in vacuum.

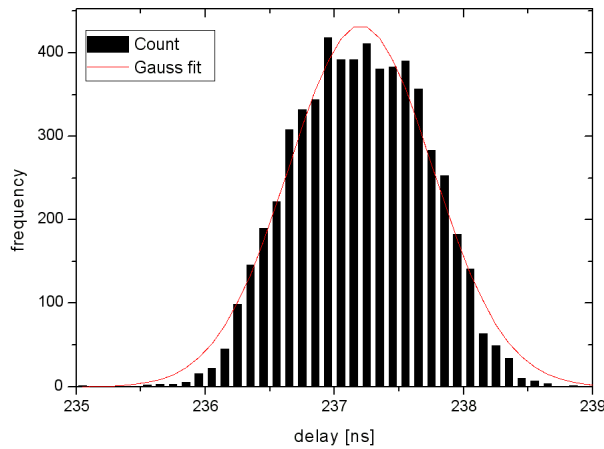


Figure 3.15.: The frequency with which certain times of delay occurred between a signal sent via the microwave link and a signal running through a coaxial cable from Alice to Bob. The overall time, the scan was running, is about 16 hours.

during about 16 hours the root mean square deviation of the delay is about 2.2 ns.

That the observed fluctuations of the delay time are larger than the predicted variation of maximally 1 ns is probably due to intrinsic jitter of our electronic equipment. The results show, however, that the change in the delay over a period comparable to the duration of a teleportation measurement is much less than the used coincidence window (about 30 ns on Bob's side) and therefore neglectable.

The setup for the measurement of the delay is shown in figure 3.16. A function generator produces a series of TTL pulses of about 200 ns width in tunable intervals. These pulses are then split in two by a T-connector. One of the resulting pulses is sent via the classical channel, the other one via the coaxial cable run through the Düker. On Bob's side both signals are processed with a Stanford SR-620 counter, which is able to measure the time difference between two signals with an accuracy in the order of 10^{-11} seconds. This delay is then read out via GPIB by a Labview VI (see appendix B.2).

3.3.4. Coding Alice's information for transmission on the classical channel

The purpose of the classical channel in teleportation is to send Bob the result of Alice's BSA. Since the BSA we are using is not complete but can discriminate only two of the Bell states, the information we have to send over the classical channel is only one bit per teleported photon. The encoding and decoding of this information is performed by high frequency electronic devices especially

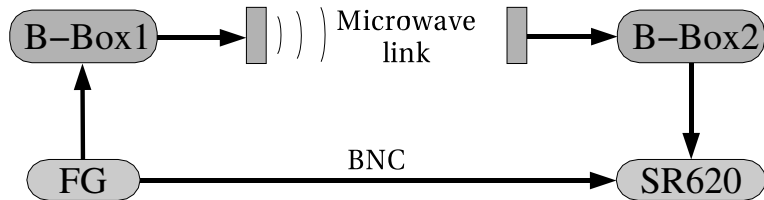


Figure 3.16.: A function generator sends one TTL pulse to B-Box1 (see next subsection) and simultaneously it sends another one directly to Bob's laboratory via a coaxial cable running below the Danube along the quantum channel. B-Box1 encodes the TTL pulse in a way processable for the microwave transmitter. This signal is then sent to Bob's side via the microwave link. There it is interpreted back into a normal TTL signal by B-Box2 and forwarded to a SR620 counter, which is counting the delay in the arrival times between the two arriving signals.

designed for this very purpose, dubbed "Bobby"-boxes¹⁷. Let us denote the encoder as "B-Box1" and the decoder as "B-Box2".

Figure 3.17 shows the scheme of this process. Alice's BSA gives three possible outcomes (ignoring any noise); it is either Ψ^- or Ψ^+ or one of the Φ -states. In the Φ -case Alice does not send anything to Bob, while the other two outcomes are coded by sending a TTL pulse either along one line or along another to B-Box1. If B-Box1 gets a signal on the Ψ^- -line (duration ~ 200 ns), it will generate a rectangular pulse of about 0.5 V height and a duration of about 5 ns. If, on the other hand, it receives a signal on the Ψ^+ -line, it will generate a pulse of the same type with about 1 V height. The result is then sent via the microwave link to Bob and forwarded to B-Box2.

B-Box2, however, does not simply revert the encoding of B-Box1. It has one input for the received signal and two outputs. One output is just a TTL trigger pulse, informing Bob, that a teleported photon is about to reach him. The second output is either 0 if B-Box2 received a Ψ^- signal or a constant signal of 5 V amplitude for a Ψ^+ -signal. This second signal will later decide if the Pockels cell will be switched or not, while the trigger pulse tells us, when this should happen. Exact specifications and circuit diagrams will be included in Rupert Ursin's PhD-thesis.

Apart from encoding, the Bobby-boxes are also a kind of translator between our detectors and logic circuits and the microwave link. As the signals of our detectors and logic have a width of approx. 200 ns, they are too broad for the microwave link, which is designed to deal with very short signals. Thus it would see these 200 ns signals as constant and would not transmit them correctly. As the signal are steeply flanked the microwave transmitter would send a signal once for the first (the rising) edge of the signal and another one for the second (the falling) edge.

¹⁷Abi Babak, the engineer who constructed them, was nicknamed Bobby.

3. Long distance quantum state teleportation

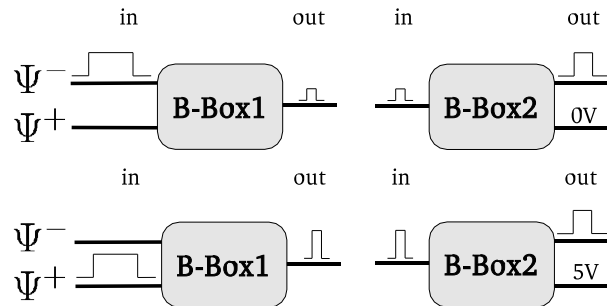


Figure 3.17.: B-Box1 generates a 0.5 V or a 1 V pulse depending on if it gets a TTL pulse on the Ψ^- or the Ψ^+ line. This pulse is then sent to B-Box2, which has to decode the information again. First, whatever pulse it gets, B-Box2 generates a trigger TTL pulse, informing us of the event. Additionally, it will generate a constant 5 V output if and only if the incoming signal originates from a Ψ^+ .

Additionally, while most of our devices are working with coaxial cables having a $50\ \Omega$ impedance, the microwave transmitter and receiver are working with $100\ \Omega$ impedances. Therefore, any signal coming from the $50\ \Omega$ devices would get partially reflected when entering the $100\ \Omega$ devices. The distortions of the signal produced in this way, would lead to severe noise in our measurement devices.

Because of these problems, we use the Bobby-boxes as an interface between the microwave link and the rest of our electronic devices. The B-Boxes have appropriate impedances on inputs and outputs. B-Box1 uses the signals of 200 ns width reaching it on the $50\ \Omega$ cables to generate a signal of approximately 80 ns width to send via the $100\ \Omega$ microwave link. On Bob's side, B-Box2 takes the 80 ns signal and generates an according $50\ \Omega$ TTL trigger pulse of 200 ns width.

3.4. The quantum channel

Our channel for the transmission of Bob's part of the shared entangled pair from Alice to Bob is an approximately 800 m long optical fiber, which is single mode for the wavelength of 789 nm. Due to absorption and birefringence we loose around 70% of the photons transmitted and any photon sent reaching the other end will of course have a different polarization on the outlet than it had before passing the fiber, a well known effect occurring in all fibers. It is compensated by squeezing the fiber on the receiver's end until the optical properties of the fiber are such that the transmitted photon will exit with the same polarization as it had when entering the fiber (or at least a state with a known relation to the original one).

Once this alignment is done, its stability will of course decrease with the length of the fiber. In our case of an 800 m long fiber, we even have to cope

with varying temperatures along the way and more drastic effects as movements of the fiber, either simply due to its own weight, or due to work done nearby, as the tunnel, the fiber is run through, is not our property but only provided to us by the MA30, whose workers of course still use the tunnel.

Hence, the steady control of the fiber's properties and according alignment is a central point in long distance teleportation to ensure its working. This has been dealt with by M. Lindenthal in his diploma thesis [31]. A Labview program was designed to measure the changes in photon polarization due to the fiber and to control a device squeezing the fiber accordingly as to counterbalance these effects. Measurements showed that the fiber is sufficiently stable over a time period of some hours. Therefore, in the final experiment, polarization measurements will probably be done once every few hours, and if necessary, the polarization control program will be started.

3.5. Bob's laboratory

In Bob's laboratory the necessary unitary transformation based upon Alice's BSA result is performed to finalize the teleportation protocol. Subsequently, the resulting photon's polarization is measured to determine if the teleportation process has been successful. In order to check this, Alice chooses the state, she teleports out of a discrete set of states. First she has to choose in which basis she wants to teleport: either in the HV-basis, the 45° -basis or the RL-basis¹⁸. Out of this basis she can than freely choose one of the basis states.

Now, to check if the teleportation process works, Bob has to measure the photon he receives in the same basis. If it works, Bob should always get the correct outcome of his measurement. The basis Bob measures in, is chosen by remotely rotating a disk containing one free frame, one with a half-wave plate and one with a quarter-wave plate. Depending on the rotation angle of the disk, the teleported photon will pass through one of the three frames, as indicated in fig. 3.18. The following table summarizes the function and content of the different frames of the disk:

frame nr.	content of frame	according measurement basis
1	nothing	HV-basis
2	quarter-wave plate, orientation: 45°	RL-basis
3	half-wave plate, orientation: 22.5°	45° -basis

Each time Alice changes her basis, she adjusts Bob's rotation stage accordingly via remote control, using a TCP connection and a Labview program which has yet (at the time of the submission of this thesis) to be programmed

Bob's task starts as soon as he receives a signal via the classical channel. This signal is translated by B-Box2 into a trigger TTL-pulse and a constant voltage output of 0 V or 5 V depending on the BSA outcome (see subsection 3.3.4), where 0 V stands for Ψ^- and 5 V for Ψ^+ .

¹⁸Corresponding to right and left circularly polarized light.

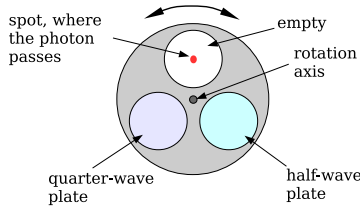


Figure 3.18.: Depending on the basis, Bob should measure in, the teleported photon is either not modified, or sent through a half-wave or a quarter-wave plate. This choice can be made by simply rotating the correct frame in the way of the photon.

As we know the time delay between the classical signal and the teleported photon (see subsection 3.3.3), the TTL pulse tells us exactly when the photon is due to arrive. On the other hand, the constant voltage output can be used as power supply for the Pockels cell's switch. Since it needs both, a 5 V power supply and a TTL pulse to trigger the switching, the Pockels cell will only be ready to switch if the constant voltage coming from the Bobby-box is 5 V. So, in this case it will be waiting for a TTL trigger to start the switching process, while for the 0 V case even the trigger will not switch it.

Accordingly, the trigger pulse must be properly delayed, as it has to trigger the Pockels cell such that it is switched when the teleported photon passes it (in the Ψ^+ -case). That means, the trigger must start the switching process about 100 ns before the photon arrives (see subsection 4.5.2). If it is triggered too late, the cell will not reach the $\lambda/2$ -voltage in time, while if it is triggered too early, the voltage may already be sinking again or at least the contrast will not be as good as at the time soon after the Pockels cell has reached the appropriate voltage.

In figure 3.19 the overall scheme is illustrated. After the photon has passed the Pockels cell it will go on straight to the polarizing beamsplitter if it is to be measured in the HV-basis. For a 45° -based measurement, it will have to go through a half-wave plate first, for a RL-based measurement, it will have to pass a quarter-wave plate, depending on the basis chosen by Alice.

After the photon has been detected, the detector signal is only counted if it arrives in coincidence with another delayed version of the TTL trigger pulse. This is necessary to ensure that we are measuring the correct photon and not just noise. It is the task of Bob's logic to check if trigger and photon detection pulse overlap. If they do, and if the photon is detected in the correct output of the PBS, this one run of the experiment has been successful.

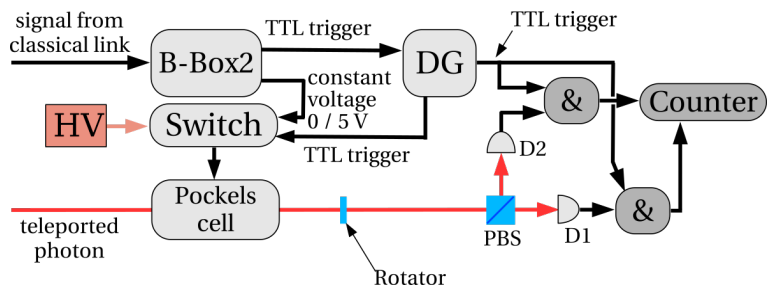


Figure 3.19.: Depending on Alice's BSA outcome, B-Box2 provides the Pockels cell with a voltage of 0 or 5 V. Only in the second case, the cell will switch as soon as the delay generator (DG) releases the TTL trigger pulse, which is also generated by B-Box2. This should happen shortly before the photon arrives. After passing the Pockels cell the correctly transformed photon is measured by the PBS, whose basis is defined by the rotator, which is set by Alice via a TCP connection. Subsequently, the corresponding detector event is counted in coincidence with the TTL trigger pulse.

4. Hardware implementation of an actively triggered unitary transformation

A central part of the long distance teleportation project (see chapter 3) is the first realization of active switching in experiment, i.e. a unitary transformation is performed, actively triggered by the outcome of the BSA. For this purpose a fast optical retarder is needed to allow switching between performing the identity operation on a photon and acting as a half-wave plate on it. To realize that, a Pockels cell is used in combination with a fast high voltage transistor switch. This chapter describes the basics of using a Pockels cell for this purpose and preliminary experiments determining its actual switching behavior.

4.1. Optical retarders as unitary transformations

Optical retarders can be used to perform a great variety of unitary operations on the polarization states of photons. For instance, let us assume we have an optical retarder oriented at an angle θ in the HV-basis, i.e. its optical axis shall be oriented at an angle θ relative to the V-position. The appropriate basis for this setup is one state collinear to the optical axis and another state orthogonal to the first:

$$\begin{aligned} |\psi\rangle_1 &= \cos\theta|V\rangle + \sin\theta|H\rangle \\ |\psi\rangle_2 &= -\sin\theta|V\rangle + \cos\theta|H\rangle. \end{aligned} \quad (4.1)$$

Suppose the optical retarder results in a phase shift $e^{i\phi}$ on the $|\psi\rangle_2$ -part of a state, while the $|\psi\rangle_1$ -part remains unchanged. Then a general polarization state in the HV-basis will be transformed according to the following equation:

$$\begin{aligned} |\chi\rangle &= a|V\rangle + b|H\rangle \mapsto \\ |\chi'\rangle &= [a\cos^2\theta + i\alpha\sin^2\theta + b(1 - e^{i\phi})\sin\theta\cos\theta]|V\rangle + \\ &\quad + [a(1 - e^{i\phi})\sin\theta\cos\theta + b\sin^2\theta + ib\cos^2\theta]|H\rangle. \end{aligned} \quad (4.2)$$

This corresponds to a transformation matrix of the form

$$\begin{pmatrix} \cos^2\theta + e^{i\phi}\sin^2\theta & (1 - e^{i\phi})\sin\theta\cos\theta \\ (1 - e^{i\phi})\sin\theta\cos\theta & \sin^2\theta + e^{i\phi}\cos^2\theta \end{pmatrix} \quad (4.3)$$

One can easily see, that performing such transformations in series results in a quite general unitary transformation. We are, however, only interested in the four unitary transformations which Bob has to perform in the standard

teleportation scheme (see subsection 2.2.2). These transformations can all be very easily realized as indicated in the following table, where $\text{hw}(0)$ describes a half-wave plate with $\theta = 0^\circ$ and $\text{hw}(45)$ accordingly one with $\theta = 45^\circ$:

outcome of BSA	Bob's transformation	realization
$ \Psi^-\rangle$	$\begin{pmatrix} -1 & 0 \\ 0 & -1 \end{pmatrix}$	identity ($\phi = 0$)
$ \Psi^+\rangle$	$\begin{pmatrix} -1 & 0 \\ 0 & 1 \end{pmatrix}$	$\text{hw}(0)$
$ \Phi^-\rangle$	$\begin{pmatrix} 0 & 1 \\ 1 & 0 \end{pmatrix}$	$\text{hw}(45)$
$ \Phi^+\rangle$	$\begin{pmatrix} 0 & 1 \\ -1 & 0 \end{pmatrix}$	first $\text{hw}(45)$ then $\text{hw}(0)$

In the first case (BSA-outcome ψ^-) nothing has to be done as the transformation is just a multiple of the identity, while in the last case (BSA-outcome ϕ^+) two half-wave plates have to be applied in series.

This way, just by using half-wave plates, Bob can perform any one of the four transformations necessary for the standard teleportation scheme. As, in the case of the long distance quantum state teleportation experiment, Alice does not perform a complete BSA but rather a more complete BSA (see section 3.2.1), in experiment Bob only has to do one of the two transformations corresponding to the outcomes ψ^- and ψ^+ . Therefore, Bob has either to do nothing ($\phi = 0$) or he has to apply a half-wave plate with $\theta = 0^\circ$ depending on Alice's BSA-outcome to transform the received state into the teleported state. Exactly this is done by a correctly adjusted Pockels-cell which can be switched between $\phi = 0$ and $\phi = \pi$ (corresponding to a half-wave plate) by applying certain levels of high voltage.

4.2. The Pockels effect

The Pockels effect is a linear electro-optical effect as discovered by Röntgen for quartz and first thoroughly investigated in several crystals by F. Pockels around 1900 [38, 39]. It occurs in anisotropic piezoelectric materials if an electric field is applied to the crystal which produces a linear change in the optical indicatrix (i.e. the inverse of the dielectric tensor) ϵ_{ij}^{-1} [26]

$$\Delta \left(\frac{1}{n^2} \right)_{ij} = \Delta \left(\frac{1}{\epsilon} \right)_{ij} = r_{ijk} E_k \quad (4.4)$$

along the axis parallel to which it is applied. Here, r_{ijk} are the Pockels coefficients. Because ϵ_{ij}^{-1} is symmetric, r_{ijk} also is symmetric in its last two indices.

To shorten the notation one can introduce new indices for the indicatrix¹, resulting in

$$\begin{pmatrix} \Delta(1/\epsilon)_1 \\ \Delta(1/\epsilon)_2 \\ \Delta(1/\epsilon)_3 \\ \Delta(1/\epsilon)_4 \\ \Delta(1/\epsilon)_5 \\ \Delta(1/\epsilon)_6 \end{pmatrix} = \begin{pmatrix} r_{11} & r_{12} & r_{13} \\ r_{21} & r_{22} & r_{23} \\ r_{31} & r_{32} & r_{33} \\ r_{41} & r_{42} & r_{43} \\ r_{51} & r_{52} & r_{53} \\ r_{61} & r_{62} & r_{63} \end{pmatrix} \begin{pmatrix} E_1 \\ E_2 \\ E_3 \end{pmatrix} \quad (4.5)$$

For a KDP crystal as we use it (see next section) there are three non-zero components of the Pockels coefficients tensor. By inserting these non-zero components in equ. (4.4) one obtains

$$\frac{x^2}{n_o^2} + \frac{y^2}{n_o^2} + \frac{z^2}{n_e^2} + 2r_{41}E_x y z + 2r_{41}E_y x z + 2r_{63}E_z x y = 1, \quad (4.6)$$

where index e denotes the extraordinary axes and o the ordinary one, assuming that our crystal is uniaxial as it was in the experiment.

To simplify this, we can assume the external field \vec{E} to be oriented along the z -axis. Finally, by rotating the coordinate system by 45° around the z -axis, and thus performing the transformation $x \rightarrow (x' - y')/\sqrt{2}$, $y \rightarrow (x' + y')/\sqrt{2}$ and $z \rightarrow z'$, we arrive at the following diagonalized form of the indicatrix

$$\left(\frac{1}{n_o^2} + r_{63}E_3\right)x'^2 + \left(\frac{1}{n_o^2} - r_{63}E_3\right)y'^2 + \frac{z'^2}{n_e^2} = 1, \quad (4.7)$$

which is of the same form as the indicatrix of a biaxial crystal $x'^2/n_x'^2 + y'^2/n_y'^2 + z'^2/n_z'^2 = 1$, with

$$\begin{aligned} n'_x &= n_o (1 + r_{63}E_3 n_o^2)^{-\frac{1}{2}} \simeq n_o^2 - \frac{r_{63}E_3 n_o^3}{2} \\ n'_y &= n_o (1 - r_{63}E_3 n_o^2)^{-\frac{1}{2}} \simeq n_o^2 + \frac{r_{63}E_3 n_o^3}{2} \\ n'_z &= n_e. \end{aligned} \quad (4.8)$$

This we got by performing a binominal expansion up to first order in r_{63} since the changes of the refractive index due to the Pockels effect are generally orders of magnitudes smaller than the refractive index itself. One can see that the index of refraction changes linearly with the external field E (Pockels effect).

In our experiment the laser beam passes through the Pockels cell parallel to the optical axis (the z -axis in the coordinate system we are using here). Therefore, we get the relevant cross-section of the optical indicatrix just by setting $z = 0$ ($z = z'$) in equation (4.7). The resulting ellipses with and without an electric field are indicated in figure 4.1.

Orienting the Pockels cell such that the y' -axis points upwards², we can freely adjust the refractive index for vertically polarized against horizontally polarized

¹The ij indices are replaced by $11 = 1, 22 = 2, 33 = 3, 23 = 4, 13 = 5, 12 = 6$, while the k subscripts remain unchanged

²Equivalently, one could choose the x' -axis to point upwards

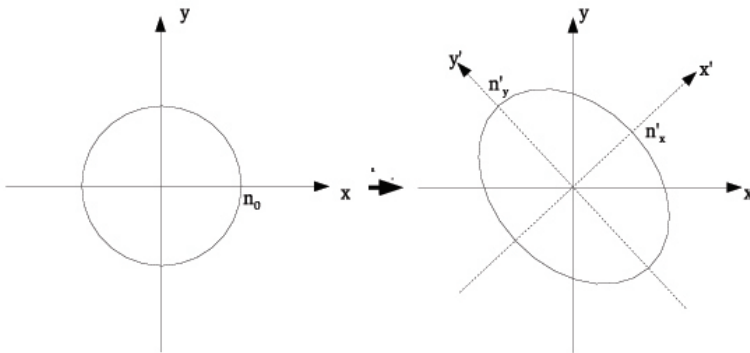


Figure 4.1.: Two cuts through the indicatrix perpendicular to the optical axis (z-axis). If no voltage is applied to the crystal, it is uniaxial and therefore the cut on the left is a circle. The ellipse on the right indicates the change of the indicatrix when voltage is applied along the z-axis. In this case the crystal becomes birefringent.

light by tuning the electric field accordingly. From equation (4.8) it follows:

$$\Delta n \equiv n'_2 - n'_1 \simeq r_{63}n_o^3 E_3. \quad (4.9)$$

Using this and taking E_3 to be U/h , where h is the height of the crystal along the optical axis and U the voltage applied to it, we get

$$\Delta n \simeq r_{63}n_o^3 U/h. \quad (4.10)$$

Since the beam's path is parallel to the optical axis and the direction the voltage is applied, the distance the light goes through the crystal is also given by h . Therefore, the total phase shift between a horizontally and a vertically polarized wave induced by the difference in the refraction indices will be $h\Delta n$. From this it follows that the voltage necessary to create a phase shift of $\lambda/2$ is given by

$$U_{\lambda/2} \simeq \frac{\lambda}{2r_{63}n_o^3}. \quad (4.11)$$

In this case, the Pockels cell acts just like a common half-wave plate in HV-orientation.

4.3. Specifications of the Pockels cell

The Pockels cell we used was a DPZ 8 model from LINOS Photonics Inc. The specifications are³:

³At a wavelength of 1064 nm and 20°C.

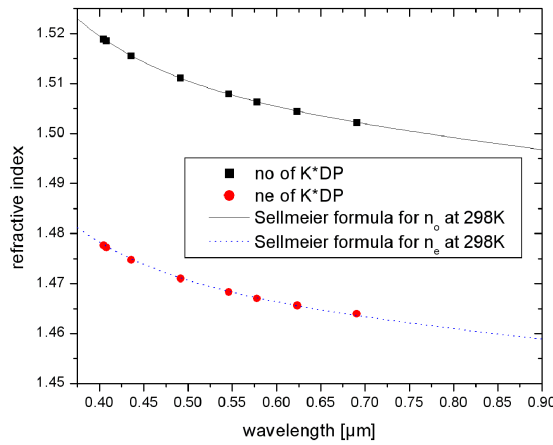


Figure 4.2.: Ordinary and extraordinary indices of refraction for KD^*P for different wavelengths and the predicted curves according to the Sellmeier formula taken from [19] for KD^*P at 298 K.

Pockels cell	DPZ 8
aperture	8 mm
electro-optical crystal	KD^*P
transmission	84%
extinction ratio	1:500
$\frac{\lambda}{4}$ -voltage	1.7 kV
maximum power	> 500 MW/cm ²
capacitance	8 pF

The electro-optical crystal is Potassium Dideuterium Phosphate (KD^*P or DKDP) which is used instead of KDP (Potassium Dihydrogen Phosphate) due its lower halfwave voltage and lower absorption. Additionally, crystals with dimensions in order of centimeters are easily available. The Pockels cell used contains two crystals mounted optically in series while electrically in parallel to provide a halving of the $\frac{\lambda}{2}$ -voltage compared to a single crystal unit and also a compensation of effects due to changes in the temperature (expansion, etc.).

In figure 4.2 the refractive indices for KDP at room temperature ($\sim 22^\circ$) are plotted⁴. As we are working with different wavelengths⁵, than those the data has been taken for, we used Sellmeier's formulas [19] for KD^*P at 298 K to calculate the according refractive indices⁶:

⁴Data taken from Cleveland Crystals, Inc. - <http://www.clevelandcrystals.com/KDP.shtml>

⁵For alignment we used a 630 nm He-Ne laser, while we used a 785 nm diode for the actual measurements, as this is nearer to the wavelength of the photons in long distance teleportation, which is ~ 789 nm

⁶The refractive indices are calculated to the third decimal in order to determine the halfwave voltage accurately up to less than 10 V.

wavelength	n_o	n_e
630 nm	1.504	1.465
785 nm	1.500	1.461

Putting this and the r_{63} -coefficient⁷ for KD^*P , $r_{63} \simeq 23 \text{ pmV}^{-1}$, in equation (4.11), we get the following $\lambda/2$ -voltages for our wavelengths:

wavelength	$U_{\lambda/2}$
630 nm	$\sim 4.03 \text{ kV}$
785 nm	$\sim 5.06 \text{ kV}$

However, since our Pockels cell consists of two crystals, the actual $\lambda/2$ -voltage will be only half of the above values.

4.4. Setting up the Pockels cell as a fast phase switch

We want to use the Pockels cell as a switchable $\lambda/2$ -plate for single photons (789 nm wavelength), as will be needed for active switching in long distance quantum state teleportation (see chapter 3). For the preliminary test we used a He-Ne laser with a wavelength of 630 nm for coarse alignment of the crystal and a laser diode at 785 nm for the actual measurements. A good contrast requires an accurate alignment of the Pockels cell, such that its optical axis is parallel to the laser beam, since then, as we have seen, the Pockels cell can act as a halfwave plate when applying the according voltage.

4.4.1. Isogyre Patterns

An easy and very exact method to align the optical axis parallel to the laser beam utilizes an effect commonly used in optical mineralogy: the interference figures obtained by illuminating a birefringent crystal with convergent (focused) light. In the case of uniaxial crystals, these figures are called isogyre patterns. This method of alignment works by rotating and tilting the crystal until the isogyre pattern produced by the crystal takes a special form and position, indicating that beam and optical axis are parallel.

For the alignment a laser beam is sent through a polarizing beam splitter (PBS)⁸, such that the transmitted beam is vertically polarized. Then a polarizer is set up (the "analyzer"), whose orientation is horizontal such that a clear extinction of the beam occurs. Then the Pockels cell is inserted between the PBS and the analyzer. It is attached to a stage allowing an adjustment of all spatial degrees of freedom of the Pockels cell (see figure 4.3).

As will be explained below, isogyre patterns are not visible for parallel light beams. To achieve a divergent beam, we either have to focus our beam or to scatter it. We chose to scatter the light, because it is less effort to do so, and because we are just interested in qualitative results of this method for alignment, not in mineralogy. Although the laser beam is already scattered from

⁷Rough value taken from [27].

⁸We could have used a common polarizer, but the quality of the PBS was better.

4.4. Setting up the Pockels cell as a fast phase switch

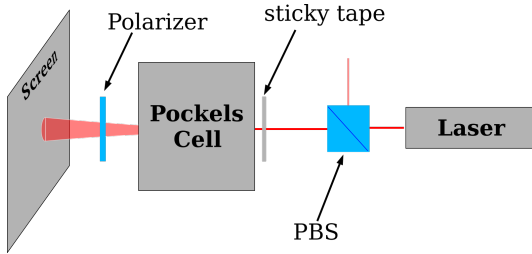


Figure 4.3.: Part of the incoming laser beam, polarized by the PBS, is scattered shortly before it enters the Pockels cell by a sticky tape. As these scattered beams are passing the Pockels cell at all possible angles, their polarization will change in general due to the birefringence of the cell. Therefore, the probability for a photon passing the second polarizer (which is crossed to the PBS) will depend on its path through the crystal resulting in according intensity variations in the spot on the screen: the isogyre pattern.

imperfections in the surfaces of our components when entering the Pockels cell, the intensity of the scattered light is still too weak to make the isogyre pattern comfortably visible. Therefore, we attached a sticky tape to the face of the Pockels cell increasing the intensity of the scattered light.

Figure 4.4 shows cross-sections of the indicatrix for different directions of propagation, assuming that the unscattered part of the laser beam is already parallel to the optical axis. For beams propagating in the vertical or in the horizontal plane the polarization does not change as in this case the E -field has only a component in either the fast or the slow axis of the crystal, depending on its initial polarization. The polarization of beams along other directions however, will have components in both the fast and the slow axis and therefore the birefringence will lead to a phase shift between the two of them.

Accordingly, light traveling along the horizontal or vertical plane will keep its polarization and will be absorbed by the analyzer, which is oriented orthogonal to the original polarization. Simultaneously, the light traveling at paths at an angle to those planes will in general acquire different polarizations and will be only partly absorbed. Due to this, the light passing the analyzer will form an isogyre pattern in the shape of a dark cross surrounded by light in the midst of which is a part of the unscattered laser beam which was not filtered out by the analyzer (see in figure 4.5). Additionally, there appear concentric dark rings in the illuminated disk, which are due to interference of light taking different paths through the crystal and thereby accumulating relative phase shifts, but they are of no relevance for the adjustment.

Thus, for perfect orientation of the laser beam along the optical axis, we expect a symmetric cross-shaped isogyre pattern. If, however, the Pockels cell is still unadjusted, we will see different isogyre patterns on the screen as illustrated in figure 4.6. When rotating and translating the cell, this isogyre pattern will change accordingly. This changing of the cell's orientation and position has

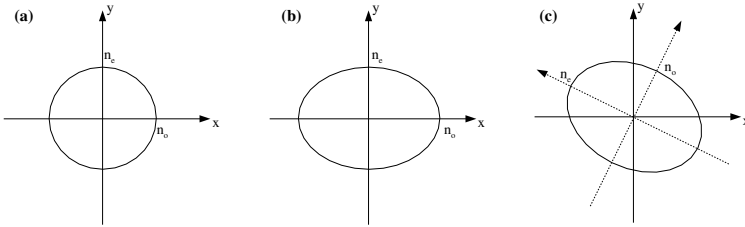


Figure 4.4.: Cuts through the indicatrix for three beams passing the crystal along different paths. For the measurements, the polarization is oriented along the x- or y-direction. (a) shows the cut for a beam lying in the plane perpendicular to the optical axis, a circle. For a beam lying in the plane containing laser beam and optical axis, the cut will in general be an ellipse with its principal axis horizontal and vertical (b). In the general case of any direction through the crystal, the cut will be a rotated ellipse (c).

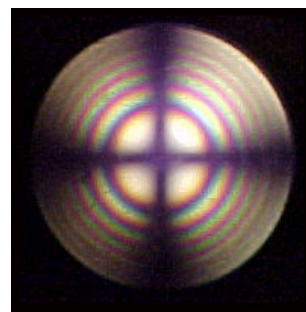


Figure 4.5.: Isogyre pattern for an uniaxial crystal (from <http://www.brocku.ca/earthsciences/people/gfinn/>).

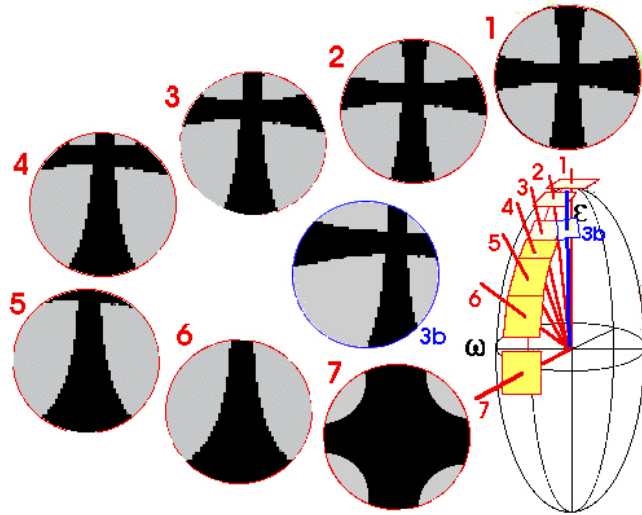


Figure 4.6.: Isogyre patterns for different orientations of the central beam relative to the optical axis. Case 1 corresponds to a well aligned Pockels cell, where the central beam is parallel to the optical axis (figure from <http://edafologia.ugr.es/>).

to be done continuously until the isogyre pattern looks like in figure 4.5 or in case 1 of figure 4.6 respectively.

4.4.2. The experimental scheme

The scheme differs only slightly from the experimental setup used for the alignment of the Pockels cell via isogyre patterns. We just remove the sticky tape to achieve a non-divergent beam and replace the polarizer after the Pockels cell with another PBS. Additionally, while it is not necessary for the alignment with the isogyre pattern, it is important for the further alignment to couple the laser light through a single mode fiber before sending it through the Pockels cell. This way, the beam is narrower and has a better beam profile for coupling into the fibers leading to the detector after the Pockels cell (for the single photon measurements later on).

The transmitted beam is sent into a photo diode to measure its intensity. Using this setup we can comfortably align the Pockels cell in such a way that it will in the end be possible to use it as a halfwave plate in the 45° basis. To achieve this, the fast and slow axis of the crystal have to be accordingly adjusted with respect to H and V.

If no voltage is applied to the Pockels cell, light will be going through it unchanged and will be transmitted by the PBS. In this case the transmitted intensity will be maximal (see figure 4.7a).

If on the other hand the $\lambda/2$ -voltage is applied to the Pockels cell, the initially vertically polarized light will acquire a $\lambda/2$ phase-shift and will leave the Pockels cell horizontally polarized. Thus, it will be reflected by the PBS and in the ideal

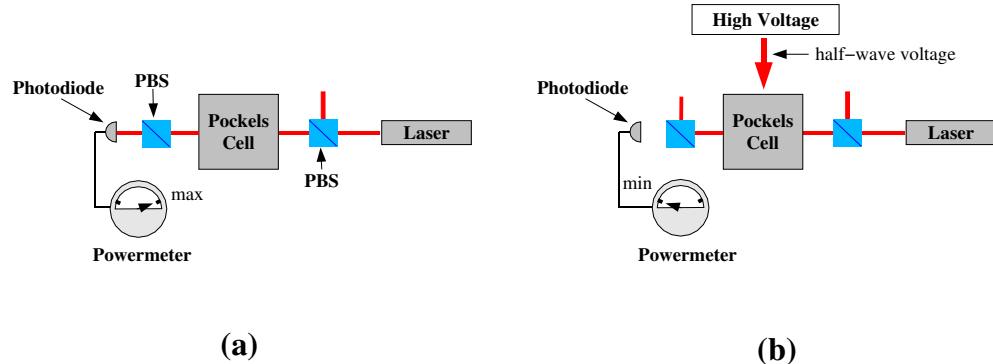


Figure 4.7.: (a) if no voltage is applied to the Pockels cell, the polarization of the laser is not changed. Therefore, nearly all of it (depending on the quality of our components) will pass through the second PBS. The photo diode should therefore measure maximum intensity in this situation. (b) if the $\lambda/2$ -voltage is applied to the cell, it will rotate the beam's polarization to horizontal. Hence, the beam will be reflected by the second PBS and the photo diode should detect minimum intensity.

case no light will reach the detector (see figure 4.7b).

Experimentally, the extinction ratio will of course be finite, as on the one hand the quality of polarizers and polarizing beam splitters is never perfect, and as on the other hand the Pockels cell will not actually behave like a perfect half-wave plate.

If the alignment following the method described in the previous section has already been done, the optical axis will be parallel to the incident beam. As a next step, one applies voltage to the crystal in order to find the $\lambda/2$ -voltage. First one can simply turn the voltage up until the transmitted intensity reaches a minimum, then the cell has to be rotated around its optical axis for optimization. Then again the voltage is tuned and so on, until a global minimum in the transmission rate is reached. When this minimum is found, the Pockels cell will be correctly adjusted for acting as a halfwave plate.

4.4.3. Specifications of the Pockels cell in static mode

Adjustments up to this moment can be either done using 630 nm light or directly using the 785 nm laser diode. In the experiment, we mostly chose to begin with red light before switching to infrared, because the basic alignment seemed to be more accurate when being done in two steps:

First, the alignment is done with red light, which is convenient as you can see the isogyre pattern and the position of the laser beam comfortably with the bare eye. This way, coarse adjustments, like centering the Pockels cell as good as possible around the laser beam and aligning the optical axis of the cell, in the beginning are very easy to do.

After aligning the position of the Pockels cell we also adjusted it roughly as a $\lambda/2$ -plate for red light by looking for the minimum intensity in the light passing the second PBS. This was done to check if the alignment was about correct, since the optimal achievable contrast and the according voltage depends very strongly of the quality of the alignment of the optical axis. Because, while the adjustment of the optical axis of the crystal never seemed to be a problem, it was not always optimal. Obviously, the human eye is not sensitive enough to distinguish more efficient orientations. Therefore, it was often necessary to make additional adjustments of the optical axis while searching the optimal voltage. This way, however, there were too many degrees of freedom involved to simply tune the parameters through. Often, one got caught in some local minimum and it was impossible to find a way out. Most of the time it proved to be the best to start the adjustment all over again to find a better minimum.

Due to this, the contrasts measured once and then again after the setup had been stripped down and built up again often differed by more than 10 or 20%. Generally one can say that with time the contrasts achieved grew higher with the experience and endurance of the experimenter.

After the alignment using red light was done, we switched to infrared light and did the same all over again but with more patience and accuracy. The single mode fiber for red light was replaced with one for infrared trying to change the direction of the laser beam as little as possible. In general after this changing of wavelength and fibers only little adjustments were necessary concerning the orientation of the optical axis. This could be done using an infrared viewer to watch the shape of the isogyre pattern and by adjusting the Pockels cell slightly in order to center the pattern again.

Then, once more, the $\lambda/2$ -voltage had to be looked for. At the end the contrast when using the Pockels cell with DC voltage, was always at least $1000 : 1$, mostly around $1500 : 1^9$. But still, the voltage to achieve this varied every time the setup was rebuilt. Therefore, the average of the contrast from setup to setup would be $(1500 \pm 200) : 1$ at a voltage of $2500 \pm 100V$. Of course, the more representative values are those measured for only one setup. However, it is a matter of patience to find the optimal setup due to the inaccuracy of the alignment of the optical axis mentioned above.

4.5. Switching the Pockels cell

In its use for active switching in teleportation the Pockels cell will have to be switched from $0 V$ to the $\lambda/2$ -voltage in a time in the order of some nanoseconds. This requires a special switch, able to cope with both, high voltages and ultra short switching times. Additionally, the fast switching should be triggered by a TTL pulse¹⁰, as will be used as indicator for the arrival of a teleported photon. The exact nature of this trigger and how it is supplied to the Pockels cell is

⁹With contrast we refer to $I_{max} : I_{min}$ the ratio of maximum and minimum intensity in the light transmitted by the analyzer.

¹⁰A "Transistor - to - Transistor - Logic" (TTL) pulse is a standardized rectangular positive pulse with a maximum amplitude of $5V$ and a minimum width of ~ 5 ns.



Figure 4.8.: Aluminium box containing both the Pockels cell and the high-voltage switch. Additionally the box has been wrapped in using a copper duct-tape.

discussed in section 3.3.4.

Due to this use of the Pockels cell as a fast switch for unitary transformations, the main attention of our experiments was paid to setting up a working rapidly switchable Pockels cell.

4.5.1. Switching high voltages on a short timescale

The switch we used was a fast high voltage transistor switch, model HTS 41-06-GSM, from Behlke Electronic GmbH. Its specifications are given in appendix A.2. The switch was placed in a small aluminum box together with the Pockels cell (see fig. 4.8). This box then was mounted on a rotation stage, which was set upon a tilting platform built upon a translation stage. A photo of the overall setup is shown in figure 4.9.

Due to the short rise and fall times of the applied voltage, the switch produces rapidly oscillating electromagnetic radiation which is then induced in the connection cables between the different devices. These induced signals distort the actual signals to be measured. Figure 4.10 shows for example the switching signal taken directly at the high voltage switch via a high voltage oscilloscope probe. Therefore, we had to take very strict precautions to prevent this radiation from influencing our data.

To achieve an accurate electromagnetic shielding, the switch together with the Pockels cell was put into a small aluminium box. This box and the stages it was

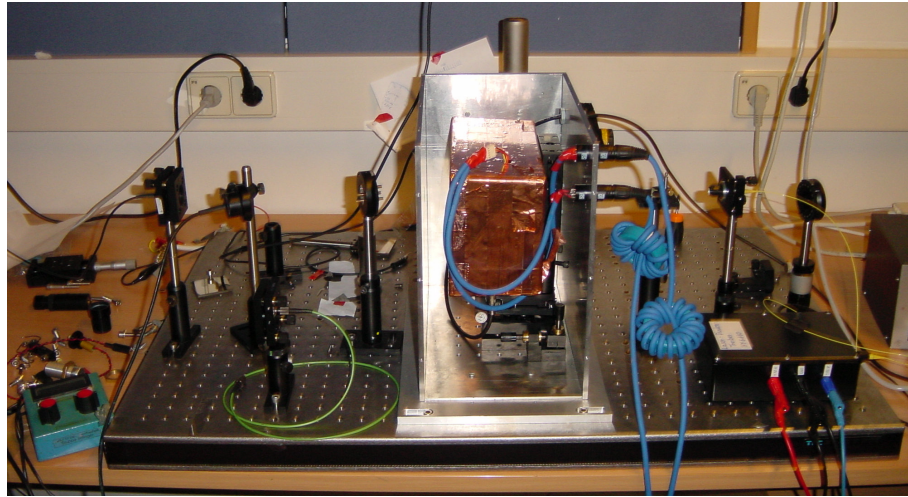


Figure 4.9.: Setup showing the Pockels cell placed in an aluminium box (additionally covered with copper) mounted on translation, tilt and rotation stages. Surrounding it, a part of the HF-shielding can be seen, opened for adjustment.

mounted on were then surrounded by a grounded aluminium box, which serves as an HF-shielding¹¹ (see photo 4.9). All these shieldings were then connected with each other on several points on their surfaces to jointly ground them. This joint grounding is essential for an HF-shield, because otherwise current will be induced in the shielding by the radiation and the oscillating currents will again produce radiation rendering the shielding useless. The realization of a usable HF-shielding was the most time-consuming part of the Pockels cell experiments. In the beginning of the experiment the grounding of the shields was far from perfect, without us realizing it. Therefore, each measurement we made, was influenced by the radiation, thus distorting the results and making us believe that there was something wrong with either the Pockels cell or the switch.

4.5.2. The switching behavior of the Pockels cell

The setup for testing the switching behavior of the Pockels cell was designed to mimic as perfectly as possible the conditions in the future active-switching experiment. Its scheme is shown in figure 4.11.

A function generator (FG) was used to generate equidistant TTL pulses as illustrated by figure 4.12 to trigger the switch. The length of a single switching event, however, was independent of the width of the TTL pulse and is always ~ 400 ns (including switching on, staying on and switching off)¹².

Each TTL pulse was then sent both to the Pockels cell and to a delay gener-

¹¹In the teleportation experiment, this box will be replaced by a box made of copper, as aluminium oxidizes very rapidly when exposed to air, lessening its conductivity on the surfaces and thus reducing the HF-shield effect.

¹²Value taken from the specifications of the switch.

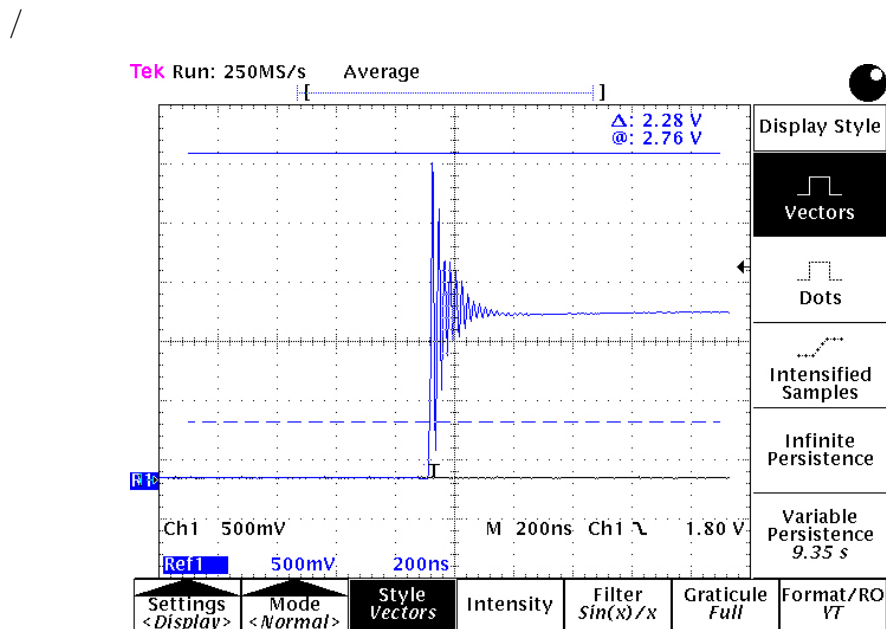


Figure 4.10.: The picture shows the voltage taken directly off the output of the fast high voltage transistor switch. 1 mV on the screen corresponds to 1 V at the switch. Due to the missing HF shield or the bad grounding respectively, the voltage oscillates heavily for more than 200 ns.

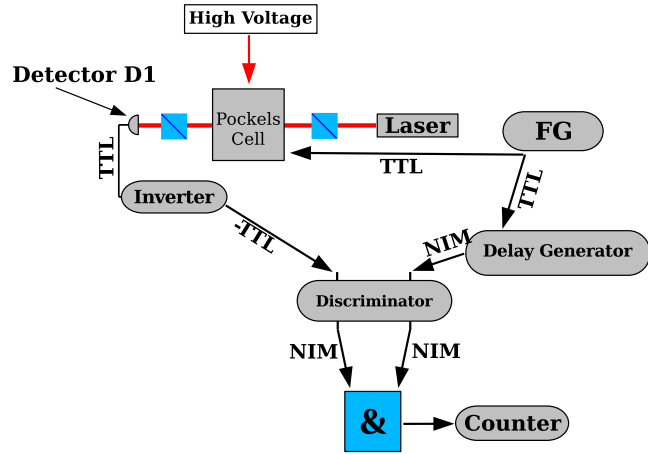


Figure 4.11.: Measuring the switching behavior of the Pockels cell: the TTL pulses needed to trigger the high voltage switch controlling the Pockels cell are generated by a function generator. Additionally, the switch has to be supplied with 5 V voltage. Depending on the voltage applied to the Pockels cell, the count rates detected by the single photon detector D1 will change from maximum (no voltage) to minimum ($\lambda/2$ -voltage). Pulses generated by D1 are only counted if they coincide with a TTL pulse delayed by an arbitrary time by the delay generator. The delayed signal thus indicates the presence of a photon in the Pockels cell. If the delay is set properly, each coincidence detection event will correspond to an actively phase-shifted photon. This enables us to get time dependent count rates illustrating the switching process of the Pockels cell.

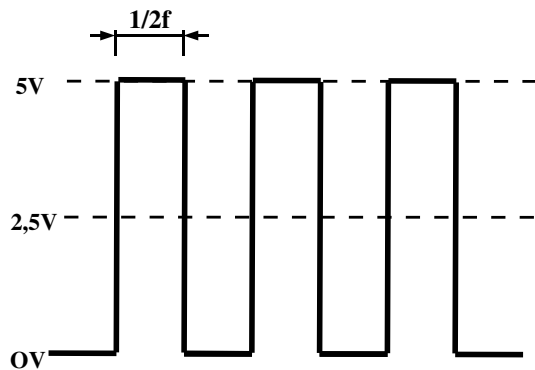


Figure 4.12.: The TTL signals triggering the switching process are generated via a function generator by simply generating a rectangular wave with a tunable frequency and 5 V amplitude. The frequency f could be freely adjusted.

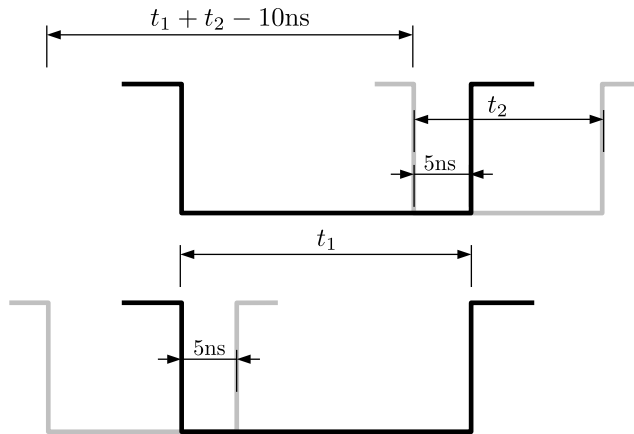


Figure 4.13.: A coincidence between two NIM signals is detected if the signals overlap for more than 5 ns. From the two cases with minimum overlap the effective coincidence window results in $t_1 + t_2 - 10\text{ ns}$.

ator (DG), which could delay the signal by any time between some picoseconds and one second. In fact, the output of the DG is triggered on the incoming TTL and puts out a new signal after the time it is told. We used the DG to produce a NIM signal¹³ after the specified period of time.

When the TTL signal reaches the high voltage switch it triggers the switch as soon as it surpasses the internal trigger threshold of the switch ($\sim 2\text{ V}$). Within a time Δt_s , which will be discussed later on, the output voltage of the switch reaches the high voltage lying on its input, which will in the ideal case be exactly the $\lambda/2$ voltage of the Pockels cell for the time of duration of the TTL-pulse. While the triggering TTL pulse's voltage stays above the 2 V threshold, the switch will hold the high output voltage. During this time the count rates at the single photon detector $D1$ (see figure 4.11) should be at a minimum if the Pockels cell has been adjusted correctly.

The TTL signals produced by detector $D1$ are inverted by a signal inverter and then enter a discriminator, producing NIM signals of a tunable width when triggered. These NIM signals are forwarded to a NIM logic performing a logical AND between the NIM signal originating from the detector and the NIM signal coming from the delay generator. The signal of the delay generator is also sent through a discriminator to allow a tuning of its width.

To get a coincidence count at the NIM logic, the incoming signals have to overlap for 5 ns. Therefore, if the first incoming signal's width is t_1 and the second signal's width is t_2 , the resulting coincidence window's width will be $t_1 + t_2 - 10\text{ns}$, where the 10 ns are just two times the necessary overlap (see fig. 4.13).

¹³A NIM (Nuclear Instrument Module) signal is a fast negative electric signal used for binary communication between electronic devices. A current between -1 mA and 1 mA signals 0, while a current between -14 mA and -36 mA signals 1.

Thus, by changing the time by which the signal going through the DG is delayed, we will get only those counts of the detector which correspond to photons passing the Pockels cell at the time chosen. Using this fact, we can scan the quality of the Pockels cell's switching at any stage. In the ideal case, if the high voltage switch and the Pockels cell were responding instantly to any change in the trigger signals and the high voltage respectively, the count rates of the detector plotted over time would exactly resemble the TTL pulses used to trigger the high voltage switch.

A scan of the coincidence count rates by continuously increasing the time delay will thus provide us with information about the inertia of the switching process such as Δt_s . Additionally, we will be able to measure the contrast of the Pockels cell acting as a half wave plate at different stages of the switching process, thus getting a picture of the switching behavior of the high voltage switch and the Pockels cell.

Scanning the switching process

The single photon detector used in the experiment saturates at a frequency of approx. 300 kHz. To avoid saturation the intensity of the laser had to be tuned down accordingly by inserting filters in front of the first beamsplitter. Thus, the beam intensity was adjusted such that detector $D1$ counted only ~ 250000 photons per second while the Pockels cell was not switched.

When scanning the switching process using the delay generator to adjust the time at which we want to count photons, the time resolution of the scan is given by both the width of the detector signals (~ 200 ns) and the width of the DG-signal. The lowest width allowed by the discriminator was approximately 7 ns, but to get reasonably high count rates, we had to find optimal signal widths allowing a high time resolution while still having sensible count rates during a not too long time of measurement.

Typical count rates to be expected can be estimated with representative values for the settings used in the experiment. Usually the TTL-signals were produced with a frequency of ~ 500 Hz, detected singles were ~ 200000 s^{-1} . Therefore, using a coincidence window 40 ns wide, would lead to coincidence count rates of approx.

$$500 \times 200000 \times 4010^{-9} = 4 s^{-1}. \quad (4.12)$$

Nevertheless, the measurements took up to one day or even more (depending on the time resolution desired) for a complete scan of the switching process. Therefore, it was necessary to write a program, controlling the DG and increasing its delay time step by step, while steadily counting the photons coinciding with the coincidence window given by the delay generator (see appendix B.1).

Results

In the following, several plots of the measurement results are given and their meaning explained. It has to be emphasized that the measurements performed were not taken in an ideal laboratory but in an office room which was frequently

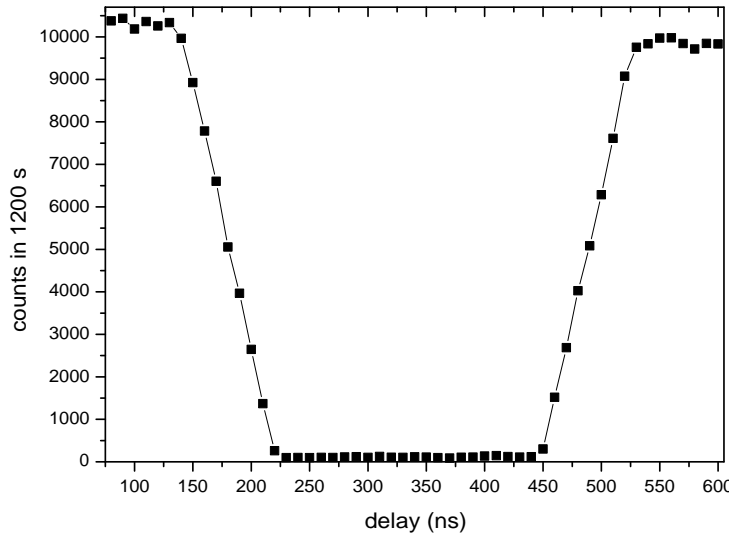


Figure 4.14.: Coincidence count rates measured at different times of delay over 1200 s. The coincidence window was ~ 35 ns, the repetition rate of the switching process was 1000 Hz, where the $\lambda/2$ -voltage was 3710 V.

entered by others, as they passed through or accessed the printer. Therefore, the dark counts were not as low as could be expected from measurements in a laboratory, although we tried to keep them as low as possible.

Figure 4.14 shows the count rates for differing times of delay. The voltage applied to the Pockels cell was 3710 V. Each count rate represents a measurement over 1200 seconds; an average of dark counts of 13 ± 3 over the time measured, has been subtracted. The width of the DG-signal was chosen to be 15 ns, while the detector pulses were set to a width of approx. 30 ns, which results in a coincidence window of ~ 35 ns. The trigger frequency was set to 1000 Hz.

The contrast for the same scan, i.e. the maximum count rates divided by the count rates at a given time of delay, is plotted in figure 4.15, where the maximum count rate has been averaged over the count rates before and after the switching process and background has been subtracted.

In order to compare the quality of the switching process as indicated by the figures 4.14 and 4.15 with the quality of our results when the HF-shield was still badly grounded, the next plots 4.16 and 4.17 were included. The first showing the count rates of one of our best scans at this time, the second the corresponding contrast.

The average dark counts given for the first picture has been calculated from the data represented in figure 4.18. It shows the dark counts during one hour

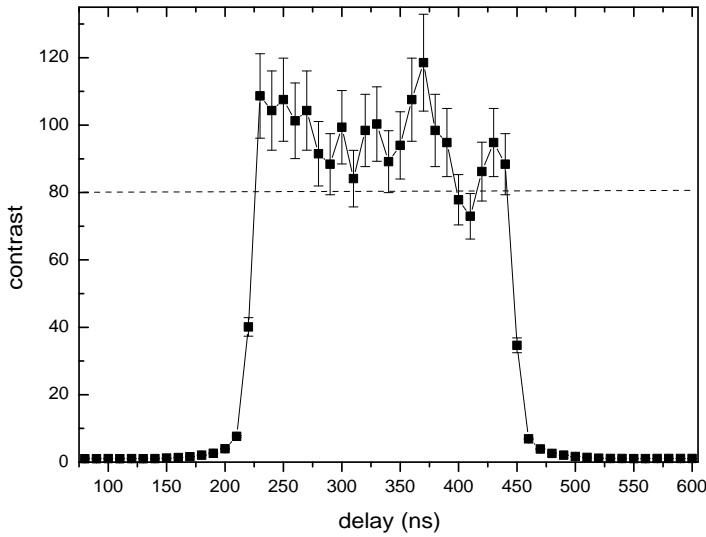


Figure 4.15.: Plot of the contrast ($N_{max}/N(t)$) for the count rates of figure 4.14.

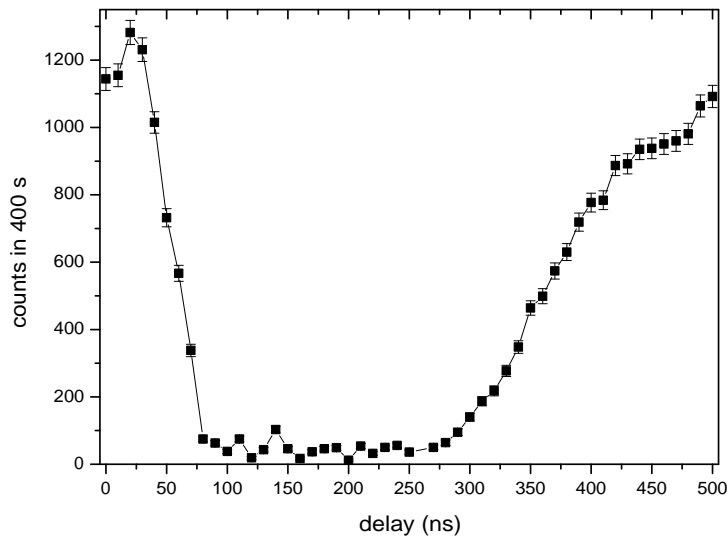


Figure 4.16.: Coincidence count rates of a former measurement where the HF-shielding was still defective.

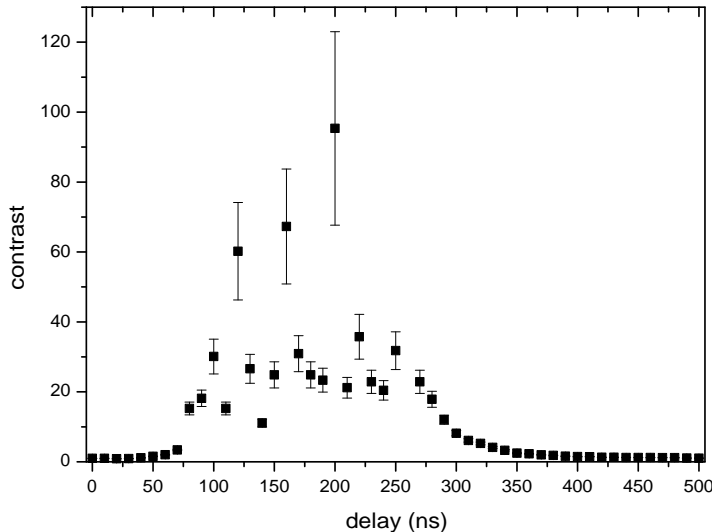


Figure 4.17.: Plot of the contrast corresponding to figure 4.16.

over a period of approximately two days, including the nights¹⁴.

Note that the dynamic contrast is well below the static contrast determined in section 4.4.3, which was always better than 1000 : 1 (often even twice as good). Also, the voltage for which this data is taken is higher compared to the DC case. When applying a static voltage to a Pockels cell, piezo electric effects occur, leading to an additional deformation of the crystal symmetries. Therefore, the $\lambda/2$ -voltage is lower than one would expect for the Pockels effect itself. For rapidly alternating voltage this additional effect is too slow to follow the changes in voltage. Thus, the piezo electric effect does not contribute to the change in birefringence of the crystal. Typically it follows, that for AC voltage the $\lambda/2$ -voltage is higher than for DC voltage by approximately 20%¹⁵.

Since, however, the adjustment procedure has been performed under DC-conditions, it was always necessary to perform an additional alignment for the operation with AC voltage. Because of the low count rates it was a far more time consuming business than for the alignment with static voltage. Unfortunately, these measurements could not be adequately performed by the use of a computer program, as the high voltage power supply could not be controlled remotely.

A typical coarse scan for the optimal voltage is given in figure 4.19 over an interval of 500 V. The corresponding contrast of the switching process for differing voltages is plotted in the figure 4.20.

The last scan performed was a scan testing the stability of the contrast over

¹⁴At one point, though, somebody seems to have switched on the light for a while.

¹⁵This value is taken from the homepage of Laser Components Inc. - http://www.lasercomponentsusa.com/app_notes_pockels_cells_q_switching.htm - a guide how to apply a Pockels cell as a Q-switch.

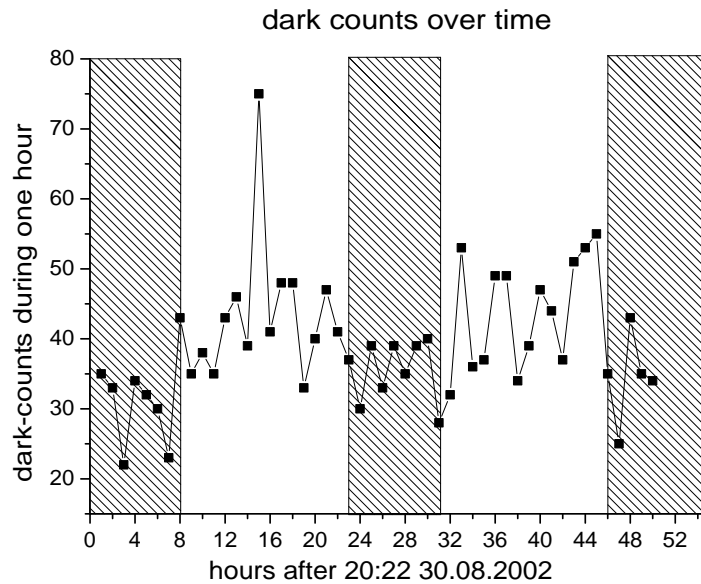


Figure 4.18.: A Scan of the dark counts per hour over roughly two days.

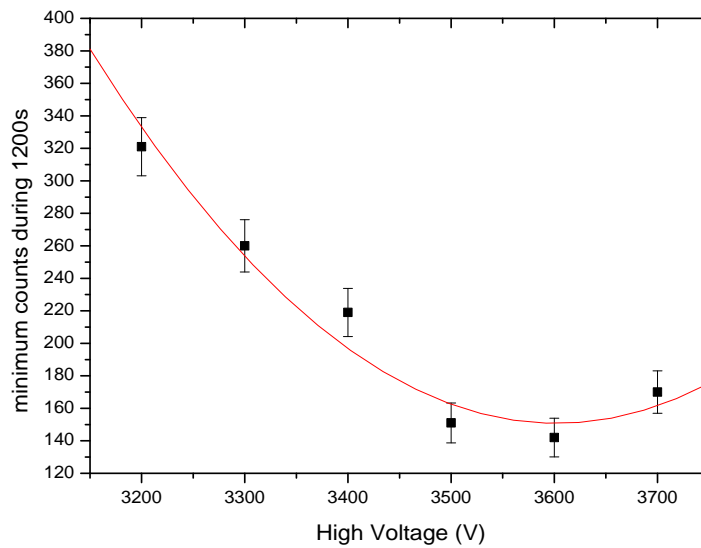


Figure 4.19.: Over an interval of 500 V coincidence counts have been measured in 100 V steps in order to scan for the optimal voltage at which the count rates would be minimal.

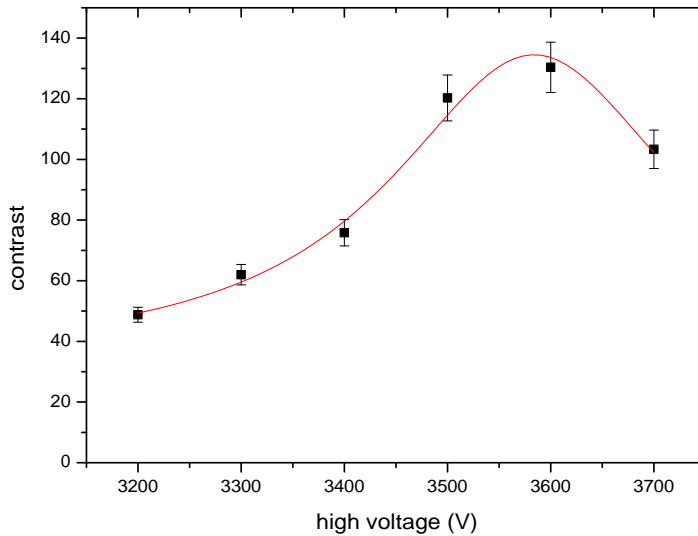


Figure 4.20.: Scan representing the contrast of the switching process at different voltages for the count rates of figure 4.19.

time for a given $\lambda/2$ -voltage. A fixed delay time at the optimum point of the switching process (i.e. short after the switching process is stabilized.) was chosen. Figure 4.21 shows the results.

Especially this last plot shows, that the contrast is never below 80 : 1 thus ensuring us, that the Pockels cell will work satisfactorily. That means, that only in one out of eighty cases when Alice measures Ψ^+ , Bob will get the wrong outcome (see chapter 3)¹⁶.

Finally, it is easy to obtain the time Δt_s (the time the switch needs from receiving the trigger signal until it is fully switched) from the measurement results. From figure 4.14 one sees that the time t_c between the delay generators setting 0 ns and the delay generator setting where the counts have finally dropped to their minimum is approximately 225 ns. However, the delay generator itself is responsible for an additional delay of about 92 ns. To this we have to add the time, the signal needs to travel through the various coaxial cables connecting the devices, which is ~ 5 ns. This results in an overall delay of ~ 322 ns.

To obtain Δt_s we have to subtract the time, the photon needs to travel from the Pockels cell to the detector, the time the detector needs to produce a corresponding TTL pulse and the time this pulse needs to reach the NIM logic, all in all ~ 75 ns. Therefore, we get

$$\Delta t_s \simeq 322 \text{ ns} - 75 \text{ ns} = 247 \text{ ns}, \quad (4.13)$$

¹⁶This would result in a teleportation fidelity of 79/80 if everything else were working perfectly.

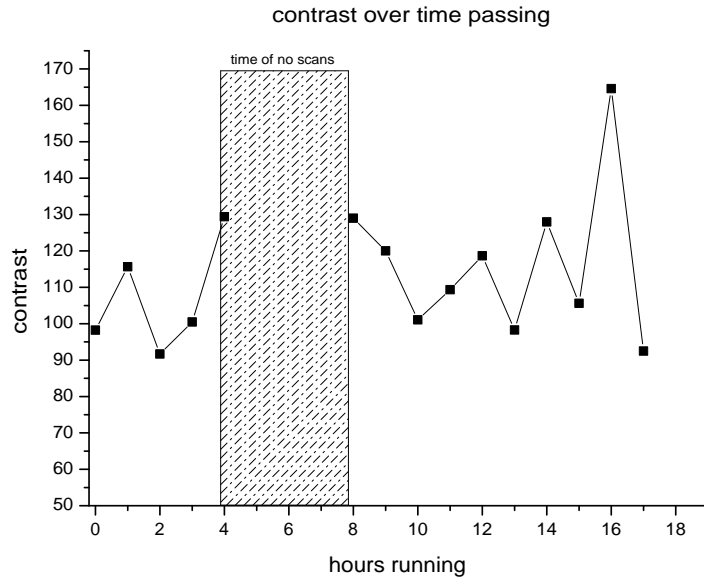


Figure 4.21.: To characterize the stability of the switching process over time, its contrast is measured over a long time. The error of each point is roughly ± 10 points on the vertical scale.

which is well below the time ($\sim 2 \mu s$) Bob has to apply his unitary transformation before the teleported photon arrives (see section 3.5).

5. Prospect and summary

Due to the rapid development of quantum information and quantum communication technology through the last years, more and more of the schemes which have been in their infancy only some years ago, are now about to become applicable in praxis, the best example being quantum cryptography. As communication mostly implies the covering of long distances, it is essential for all quantum communication schemes to test them on their applicability over such distances.

Since most quantum communication schemes are based on the use of entanglement, it is crucial to test the limits for a faithful distribution of entanglement over long distances and also to think of ways to extend these limits. A quantum repeater allows us in principle to do exactly this.

Long distance quantum state teleportation is again a step in this direction to make quantum communication schemes applicable. The experiment is going to demonstrate the teleportation of a quantum state over a real distance of about 600 meters. Simultaneously, our scheme will utilize this distance to realize the first implementation of active switching, thus going a big step in the direction of reliable teleportation¹.

The central part of this diploma thesis was the investigation of an electro optic modulator, which will be used for actively switching between the two unitary operations, which have to be applied by Bob on the received photon to finalize the teleportation process. The results of the experiments presented here show, that the electro optic modulator is well suited for this purpose. Its switching contrast, is always better than 80:1 and will probably be even better when used in proper laboratory conditions.

Subsequently, the stability of the classical link between Alice's and Bob's laboratory is discussed. It is investigated, if the changes of the refractive index of air depending on weather conditions could have any significant influence on the delay between the arrival of the teleported photon and the according classical signal. Simulations and measurements show that atmospheric propagation should not be a limiting feature for the classical link.

Additionally, the relation between nonlocality and teleportation is discussed. The interest lies in proving that high-fidelity teleportation is a quantum effect which cannot be simulated by means of local hidden variables. This is proven by violating a Bell inequality applied to the standard scheme of teleportation in contrast to a more complex scheme used by Th. Jennewein et al. Due to its

¹i.e. teleporting a state faithfully without having to test if it really worked. Only in this way, it will be possible to use teleportation as a tool in future quantum communication or quantum computing schemes.

5. Prospect and summary

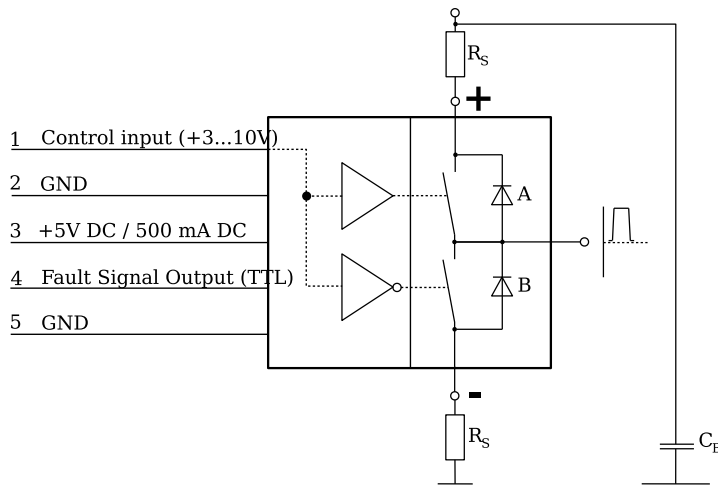
simpleness, it will be easy to test the violation of the inequality experimentally, which is planned to be done in the near future.

A. Specifications

For those, technically interested in the devices we use in the long distance teleportation project, here are the collected specifications of some of the devices mentioned in the text.

A.1. Fast high voltage transistor switch

For controlling the Pockels cell, we use a fast high voltage transistor switch type HTS 41-06-GSM from BEHLKE Electronic. The advantage of using this push-pull switch is a better control of the actual output of the switch and additionally the possibility to switch positive and negative voltages, or to switch starting from a bias voltage. We are not using these features, though, and just use it as a typical transistor switch for high voltages. The electronic circuit controlling the switch is plotted below:



For the two resistors R_S we used 22Ω resistors, the capacity is 10 nF .

A.2. Microwave link

The microwave link works in the 2.4 GHz ISM band (2.4 GHz to 2.4835 GHz) which has been subdivided by the manufacturer into 5 channels in 14 MHz steps. The original purpose of the microwave link is the transmission of audio and video data.

A. Specifications

A.2.1. Transmitter unit

Video input	Composite colour picture signal pos. $1 \pm 0.1 V_{pp}$, adjustable 0.5 – 1.5 V
Video bandwidth	30 Hz - 5 MHz
Modulation mode	Video/Audio frequency modulated F3F
Audio input	500 mV (V_{eff}) at ≤ 10 kOhm bis 10 V
Audio bandwidth	15 Hz - 20 kHz
Switching channel frequency	Audio A 32 kHz
switching channel input	10 kOhm
Power supply DC	7 to 30 V
Current demand	typical 80 mA at 12 V, max. 100 mA at 12 V
Antenna	circuit board antenna
Dimensions without antenna	180 × 120 × 70 mm
Weight without power supply	350 g
Protection class	IP 54 ¹
Ambien temperatures (use/store)	-10°C ... +55°C / -20°C ... +60°C
Air humidity	max. 70% not condensed

¹Protection against the penetration of hazardous dust deposits (dust-proof) and protection against splash water (from all directions).

A.2.2. Receiver unit

Frequency range	2.4 - 2.483 GHz
Channels	5
AFC range ²	± 3.5 MHz
Range indoor's	40-50 m
Range outdoor's	500-750 m
Video input	Composite colour picture signal pos. $1 \pm 0.1 V_{pp}$, adjustable 0.5 – 1.5 V
Video bandwidth	30 Hz - 5 MHz
Modulation mode	Video/Audio frequency modulated F3F
Audio output A and B	500 mV (V_{eff}) at ≤ 1 kOhm
Audio bandwidth	15 Hz - 16 kHz
Sensitivity noise limited	± 32 dB μ V at $SN = 12$ dB
Sensitivity gain limited	± 14 dB μ V
Switching channel frequency	Audio A 32 kHz
switching channel and AV-output	15 V / 80 mA open collector
Power supply DC	8 to 10 V
Current demand without load	320 mA, max. 100 mA at 12 V
Antenna	8 dB
Dimensions without antenna	175 × 133 × 68 mm
Weight without power supply	230 g
Protection class	IP 54 ¹
Ambien temperatures (use/store)	-10°C ... +55°C / -20°C ... +60°C
Air humidity	max. 70% not condensed

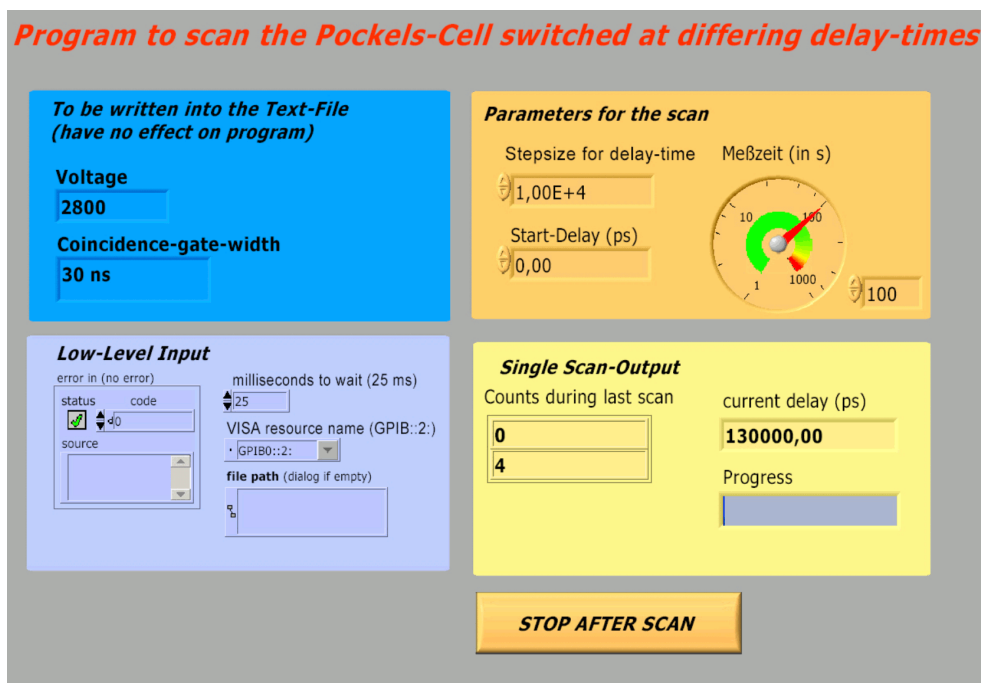
¹Protection against the penetration of hazardous dust deposits (dust-proof) and protection against splash water (from all directions).

²The automatic frequency control range determines how much the receiver frequency can differ from the transmission frequency while still being able to decipher the signal.

B. Labview programs

B.1. Scanning the switching process of the Pockels cell

For scanning the Pockels cell, it was necessary to continuously vary the delay time of the delay generator depending on where along the time line of the switching process, one wanted to count the photons registered by the detector. Additionally, these counts had to be recorded by the program by writing them to a data file. The following picture shows the panel of the program:

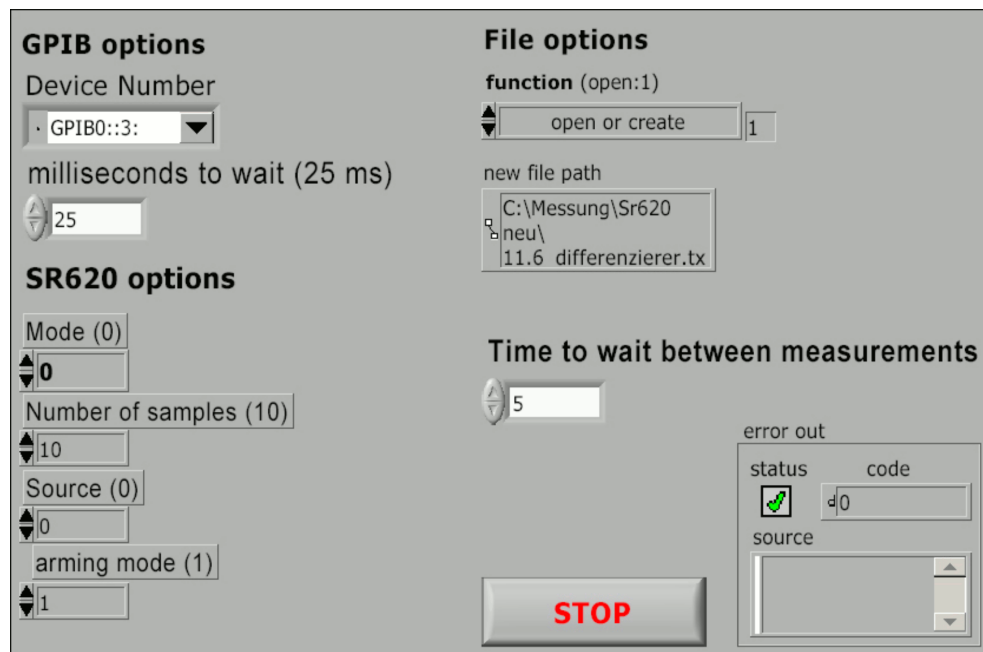


The delay generator was controlled via a GPIB interface which is standard in most of today's remote controllable measuring devices.

B.2. Measuring the time delay between classical and quantum channel

The measurements of the time delay between classical and quantum channel also required the writing of an appropriate program for reading out the SR620 counter. Again, this was done via a GPIB interface. The panel is shown in the following picture:

B. Labview programs



Bibliography

- [1] C.O. Alley and Y.H. Shih. New type of einstein-podolsky-rosen experiment using pairs of light quanta produced by optical parametric down conversion. In M. Namiki, editor, *Proc. 2nd International Symposium on Foundations of Quantum Mechanics in the Light of New Technology*, page 47, Tokyo, 1986.
- [2] A. Aspect, J. Dalibard, and G. Roger. Experimental test of Bell's inequalities using time-varying analyzers. *Phys. Rev. Lett.*, 49(25):1804–1807, 1982.
- [3] John S. Bell. On the problem of hidden variables in quantum mechanics. *Rev. Mod. Phys.*, 38:447–452, 1966.
- [4] J.S. Bell. On the Einstein Podolsky Rosen paradox. *Physics*, 1:195–200, 1964.
- [5] C. H. Bennett, G. Brassard, and N. D. Mermin. Quantum cryptography without bell's theorem. *Phys. Rev. Lett.*, 68:557–559, 1992.
- [6] Charles H. Bennett, Gilles Brassard, Claude Crépeau, Richard Jozsa, Asher Peres, and William K.Wootters. Teleporting an unknown quantum state via dual classical and Einstein-Podolsky-Rosen channels. *Phys. Rev. Lett.*, 70(13):1895–1899, 1993.
- [7] Charles H. Bennett and Stephen J. Wiesner. Communication via one- and two-particle operators on Einstein-Podolsky-Rosen states. *Phys. Rev. Lett.*, 69(20):2881–2884, 1992.
- [8] L. A. Bloomfield. *How things work*. John Wiley & Sons, Inc., 1997.
- [9] D. Bohm. A suggested interpretation of the quantum theory in terms of “hidden” variables. I. *Phys. Rev.*, 85(2):166–179, 1952.
- [10] D. Bohm. A suggested interpretation of the quantum theory in terms of “hidden” variables. II. *Phys. Rev.*, 85(2):180–193, 1952.
- [11] David Bohm and Yakir Aharonov. Discussion of experimental proof for the paradox of Einstein, Rosen, and Podolsky. *Phys. Rev.*, 108(4):1070–1076, 1957.
- [12] N. Bohr. Can quantum-mechanical description of physical reality be considered complete? *Phys. Rev.*, 48:696–702, 1935.

Bibliography

- [13] D. Boschi, S. Branca, F. De-Martini, L. Hardy, and S. Popescu. Experimental realization of teleporting an unknown pure quantum state via dual classical and Einstein-Podolsky-Rosen channels. *Phys. Rev. Lett.*, 80:1121–1125, 1998.
- [14] D. Bouwmeester, J.-W. Pan, K. Mattle, M. Eibl, H. Weinfurter, and A. Zeilinger. Experimental quantum teleportation. *Nature*, 390:575–579, 1997.
- [15] S. Braunstein and A. Mann. Measurement of the bell operator and quantum teleportation. *Phys. Rev. A*, 51:R1727–R1730, 1995.
- [16] D. C. Burnham and D. L. Weinberg. Observation of simultaneity in parametric production of optical photon pairs. *Phys. Rev. Lett.*, 25:84–7, 1970.
- [17] J. Calsamiglia and N. Lütkenhaus. Maximum efficiency of a linear-optical bell-state analyzer. *Appl. Phys. B*, 72(1):67–71, 2001.
- [18] J. F. Clauser, M. A. Horne, A. Shimony, and R. A. Holt. Proposed experiment to test local hidden-variable theories. *Phys. Rev. Lett.*, 23:880–884, 1969.
- [19] V.G. Dmitriev, G.G. Gurzadyan, and D.N. Nikogosyan. *Handbook of Non-linear Optical Crystals*. Springer, 1990.
- [20] A. Einstein, B. Podolsky, and N. Rosen. Can quantum-mechanical description of physical reality be considered complete? *Phys. Rev.*, 47:777–780, 1935.
- [21] Artur K. Ekert. Quantum cryptography based on Bell’s theorem. *Phys. Rev. Lett.*, 67(6):661, 1991.
- [22] L. Essen and K. D. Froome. The refractive indices and dielectric constants of air and its principal constituents at 24000 mc/s. *Proceedings of the Physical Society, Serie B*:216, 1951.
- [23] Richard P. Feynman. There’s plenty of room at the bottom. *Caltech’s Engineering and Science*, February 1960.
- [24] A. Furusawa, J. L. Sorensen, S. L. Braunstein, C. A. Fuchs, H. J. Kimble, and E. S. Polzik. Unconditional quantum teleportation. *Science*, 282:706–709, 1998.
- [25] R. Ghosh, C. K. Hong, Z. Y. Ou, and L. Mandel. Interference of two photons in parametric down conversion. *Phys. Rev. A*, 34(5):3962–3968, 1986.
- [26] P. Günter. *Nonlinear Optical Effects and Materials*, chapter Second-Order Nonlinear Optical Organic Materials, page 166. Springer, Heidelberg, 2000.
- [27] Eugene Hecht. *Optik*. Addison-Wesley (Deutschland) GmbH, 1989.

- [28] Thomas Jennewein. *Quantum Communication and Teleportation Experiments using Entangled Photon Pairs*. PhD thesis, Universität Wien, 2002.
- [29] Christian Kurtsiefer, Markus Oberparleiter, and Harald Weinfurter. High efficiency entangled photon pair collection in type II parametric fluorescence. quant-ph/0101074, 2001.
- [30] P. G. Kwiat, K. Mattle, H. Weinfurter, A. Zeilinger, A.V. Sergienko, and Y. Shih. New high-intensity source of polarization-entangled photon pairs. *Phys. Rev. Lett.*, 75:4337–4341, 1995.
- [31] Michael Lindenthal. Polarisationsstabilität in einem Quantenteleportationsexperiment über große Entfernung. Master’s thesis, Universität Wien, 1997.
- [32] N. Lütkenhaus, J. Calsamiglia, and K.-A. Suominen. Bell measurements for teleportation. *Phys. Rev. A*, 59:3295–3300, 1999.
- [33] Klaus Mattle, Harald Weinfurter, Paul G. Kwiat, and Anton Zeilinger. Dense coding in experimental quantum communication. *Phys. Rev. Lett.*, 76(25):4656–4659, 1996.
- [34] J. Von Neumann. *Mathematische Grundlagen der Quantenmechanik*. Springer, Berlin, 1932.
- [35] Z. Y. Ou, C. K. Hong, and L. Mandel. Violation of locality in correlation measurements with a beamsplitter. *Phys. Lett. A*, 122(1):11–13, 1987.
- [36] Z. Y. Ou and L. Mandel. Violation of Bell’s inequality and classical probability in a two-photon correlation experiment. *Phys. Rev. Lett.*, 61(50):50–53, 1988.
- [37] James C. Owens. Optical refractive index of air: Dependence on pressure, temperature and composition. *Appl. Opt.*, 6(1):51–59, January 1967.
- [38] Friedrich Pockels. *Göttinger Abhandlungen 39*. 1894.
- [39] Friedrich Pockels. *Lehrbuch der Kristalloptik*. Leipzig, 1906.
- [40] C. D. Dermer R. J. Murphy and R. Ramaty. High energy processes in solar flares. *ApJ (Suppl.)*, 63:721, 1987.
- [41] M. A. Rowe, D. Kielpinski, V. Meyer, C. A. Sackett, W. M. Itano, C. Monroe, and D. J. Wineland. Experimental violation of a bell’s inequality with efficient detection. *Nature*, 409:791 – 794, 2001.
- [42] Terry Rudolph and Barry C. Sanders. Requirement of optical coherence for continuous-variable quantum teleportation. *Phys. Rev. Lett.*, 87(077903), 2001.
- [43] Erwin Schrödinger. Discussion of probability relations between separated systems. *Proceedings of the Cambridge Philosophical Society*, 31:555–562, 1935.

Bibliography

- [44] C. E. Shannon. A mathematical theory of communication. *The Bell System Technical Journal*, 27:379–423,623–656, July,October 1948.
- [45] Gordon D. Thayer. An improved equation for the radio refractive index of air. *Radio Science*, 9(10):803–807, October 1974.
- [46] Lev Vaidman and Nadav Yoran. Methods for reliable teleportation. *Phys. Rev. A*, 59:116–125, 1999.
- [47] G. Weihs, T. Jennewein, C. Simon, H. Weinfurter, and A. Zeilinger. Violation of Bell’s inequality under strict Einstein locality conditions. *Phys. Rev. Lett.*, 81:5039–5043, 1998.
- [48] Gregor Weihs. *Ein Experiment Zum Test der Bellschen Ungleichung unter Einsteinscher Lokalität*. PhD thesis, Universität Wien, 1999.
- [49] W. K. Wootters and W. H. Zurek. A single quantum cannot be cloned. *Nature*, 299:802–803, 1982.

Curriculum Vitae

- 31.08.1979 Born in St. Pölten.
- 1985–1989 Volksschule (Primary School) in Göpfritz/Wild
- 1989–1997 Realgymnasium (Highschool) in Waidhofen/Thaya
- 1998 Military service in the Austrian military forces
- 1998–2003 study of theoretical physics at the University of Vienna
- 2002–now research as a member of Anton Zeilinger's group for Quantum Experiments and the Foundations of Physics
- 2003 diploma thesis in experimental physics

Acknowledgments

My sincere **THANKS** go to

- my **parents** for allowing me to choose freely whatever there was to choose.
- **Prof. Anton Zeilinger** for giving me the chance to work in this fascinating new branch of physics and for the great conditions under which this is possible here in his group.
- my tutor **Dr. Markus Aspelmeyer** for all the inspiring discussions we had, for his vivid, lively way of keeping me on track and steadily learning and for his really sparse time he gave me so much of.
- the **University of Vienna** for the great facilities they offer to our group and for not having lost me along my studies.
- **Prof. Markus Arndt**, without whom I would not have started my diploma thesis with this group and without whom I would probably have turned away from physics altogether.
- **Thomas Bauer** for being a great friend and for not throwing me out of our flat all the times I did not wash our dishes due to my work.
- my colleagues **Thomas Jennewein, Rupert Ursin, Caslav Brukner** for their know how and brilliant discussions.
- my fellow diploma students **Michael Lindenthal** and **Hannes Böhm** for their friendship and the great atmosphere while going this way together.
- **Georg Oppitz** for making the first year of studying worthwhile, not just bearable.
- my **sister**, my **brother** and all the **friends** who accompanied me through all these years and who would certainly deserve more to be written about them than I could fit one this page.